Journal of Colloid and Interface Science 654 (2024) 390–404

Contents lists available at ScienceDirect

Journal of Colloid And Interface Science

journal homepage: www.elsevier.com/locate/jcis

Gold nanoparticle adsorption alters the cell stiffness and cell wall bio-chemical landscape of *Candida albicans* fungal cells

Rowan Penman [a], Rashad Kariuki [a], Z.L. Shaw [b], Chaitali Dekiwadia [c], Andrew J. Christofferson [a], Gary Bryant [a], Jitraporn Vongsvivut [d], Saffron J. Bryant [a,*], Aaron Elbourne [a,*]

[a] School of Science, STEM College, RMIT University, Melbourne, VIC 3001, Australia
[b] School of Engineering, STEM College, RMIT University, Melbourne, VIC 3001, Australia
[c] RMIT Microscopy and Microanalysis Facility (RMMF), RMIT University, Melbourne, Victoria 3001, Australia
[d] Infrared Microspectroscopy (IRM) Beamline, ANSTO – Australian Synchrotron, Clayton, VIC 3168, Australia

GRAPHICAL ABSTRACT

Citrate capped 100 nm Gold Nanoparticle Adsorption is shown to Alters the Cell Stiffness and Cell wall Bio-Chemical Landscape of Candida albicans Fungal Cells.

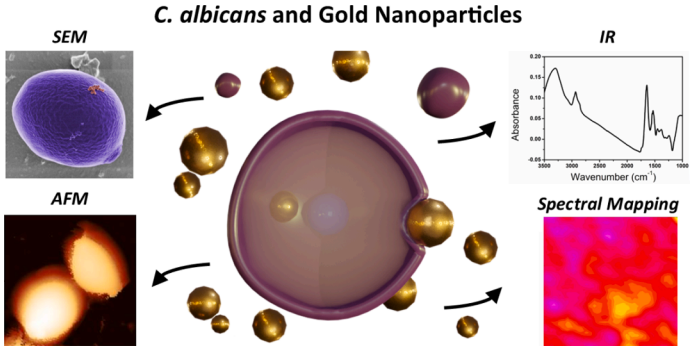

ARTICLE INFO

Keywords:
Fungi
Nanoparticle
Atomic force microscope
Synchrotron
Macro attenuated total reflection-FTIR

ABSTRACT

Hypothesis: Nanomaterials have been extensively investigated for a wide range of biomedical applications, including as antimicrobial agents, drug delivery vehicles, and diagnostic devices. The commonality between these biomedical applications is the necessity for the nanoparticle to interact with or pass through the cellular wall and membrane. Cell-nanomaterial interactions/uptake can occur in various ways, including adhering to the cell wall, forming aggregates on the surface, becoming absorbed within the cell wall itself, or transversing into the cell cytoplasm. These interactions are common to mammalian cells, bacteria, and yeast cells. This variety of interactions can cause changes to the integrity of the cell wall and the cell overall, but the precise mechanisms underpinning such interactions remain poorly understood. Here, we investigate the interaction between commonly investigated gold nanoparticles (AuNPs) and the cell wall/membrane of a model fungal cell to explore the general effects of interaction and uptake.
Experiments: The interactions between 100 nm citrate-capped AuNPs and the cell wall of *Candida albicans* fungal cells were studied using a range of advanced microscopy techniques, including atomic force microscopy, confocal

* Corresponding authors.
E-mail addresses: saffron.bryant@rmit.edu.au (S.J. Bryant), aaron.elbourne@rmit.edu.au (A. Elbourne).

https://doi.org/10.1016/j.jcis.2023.10.017
Received 31 July 2023; Received in revised form 8 September 2023; Accepted 4 October 2023
Available online 6 October 2023

laser scanning microscopy, scanning electron microscopy, transmission electron microscopy, and synchrotron-FTIR micro-spectroscopy.
Findings: In most cases, particles adhered on the cell surface, although instances of particles being up-taken into the cell cytoplasm and localised within the cell wall and membrane were also observed. There was a measurable increase in the stiffness of the fungal cell after AuNPs were introduced. Analysis of the synchrotron-FTIR data showed significant changes in spectral features associated with phospholipids and proteins after exposure to AuNPs.

1. Introduction

The field of nanomedicine is rapidly expanding, with nanomaterials finding use in a number of applications, including drug delivery [1], biosensing [2], disease detection [3], and antimicrobials [1,4], amongst others [2,5,6]. The commonality between all bio-nanomaterials is that they must interact with a biological entity via the bio-interface (including cell wall, outer and inner membrane, and lipid bilayer) – the barrier which separates the organism, or bio-construct, from the external environment [7–12]. Nanomaterials can interact with the bio-interface in a number of different ways [4,13–18], including adhesion, adsorption, surface aggregation, membrane/cell wall encapsulation [1,3,19], and cell translocation [20]. These interactions can lead to notable biophysical, biochemical, and morphological changes, which may cause changes to the integrity of the bio-interface itself [3,21,22], and in some cases, result in cell death [1,4]. Despite this, the precise mechanisms underpinning many of these interactions and subsequent consequences remain unknown [6,13,15,16,23–28].

This is indeed true for fungal cells, where nanomaterials must interact with the fungal cell wall for use as therapeutics [20,29–34], antifouling materials [35], and theragnostic agents [36–39]. Fungi are eukaryotic microorganisms [40,41], which can exist as single-celled yeasts and/or moulds, and are of increasing scientific and health-care interest. This is because pathogenic fungi have begun developing anti-biotic and antiseptic resistance [42–44], meaning that conventional treatments are beginning to fail. In response, the scientific and medical communities have begun to investigate nanomaterials, including nano-particles and nanosheets, as next-generation therapeutic [5,23,32,33,45–50] and diagnostic agents [36,38,39]. Studies have investigated the behaviour of a variety of nanomaterials with both model systems [51,52], and live cells [53–55], as well as theoretical and computational approaches [4,52,56]. However, detailed model bio-physical and biochemical systems have not been reported at the single-cell level. In order to develop an improved understanding of the ways in which fungal cells and nanoparticles interact, it is necessary to develop model systems. Access to such systems will assist in the design, opti-misation, and implementation of novel nano-fungal-therapeutics.

In recent years, advanced electron, spectroscopic, and scanning probe techniques have emerged which can provide nanoscale physical and chemical insights into cellular entities. For instance, atomic force microscopy (AFM) is a powerful tool for the in situ imaging of live cells as it allows direct label-free imaging over relatively large areas in a liquid environment [57,58]. Many previous studies have employed AFM techniques to investigate the interactions between nanomaterials and living cell systems [53–55,59,60], as well as cellular mimics including lipid bilayers [61]. Beyond cellular imaging, AFM indentation can be readily used to probe the nanomechanical properties of living cell systems, which can provide insights into the biophysical response of an organism to a nanomaterial [59,60]. Investigation of whole *Candida albicans* (*C. albicans*) cells have shown that the Young's modulus (elasticity) of the cells can be correlated to the amount of chitin present in the cell wall, providing insights into the composition of the cell [62]. Transmission electron microscopy (TEM) is also capable of visualising the internal structures of single-celled organisms with nanometre resolution, providing insights into nanoparticle adsorption, adhesion, and/or internalization [63–68]. Biochemical changes occurring externally and within biological tissues or single-celled organisms can also readily be interrogated using Fourier transform infrared (FTIR) micro-spectroscopy [46,69–77]. To date, these techniques have not been used to evaluate the biophysical and biochemical changes which occur to fungal cells following nanoparticle interactions.

Fungi are complex eukaryotic organisms [78]. Fungal cell walls can consist of various layers containing a range of structural poly-saccharides, mannoproteins, beta-glucans, chitin, and lipids which in *C. albicans* organises into three distinct layers – 1) the cell membrane, 2) the inner cell wall, and 3) the outer cell wall (Schematic 1) [43]. The innermost layer is the cell membrane, a phospholipid bilayer that separates the cell's interior from the external environment. Surrounding the cell membrane is the inner cell wall, primarily composed of glucans and mannoproteins, providing structural support and protection. The outermost layer is the outer cell wall, comprising a fibrillar network of mannoproteins and polysaccharides, contributing to adhesion and immune evasion [8,78–81]. Understanding the complexity of the *C. albicans* cell wall and membrane is crucial when investigating nanoparticle interactions, because these structures play a vital role in determining any nanomaterial's ability to penetrate and interact with the fungal cell. These interactions ultimately determine the nanomaterial's biological utility, including in therapeutics, antimicrobials, and bio-imaging technologies.

In this work, the interactions between model gold nanoparticles (AuNPs) and fungal cells are investigated with nanoscale physical and chemical resolution. Specifically, the biochemical and biophysical interactions of 100-nm-diameter citrate-capped AuNPs and a model fungal cell, *C. albicans*, were studied using a range of advanced microscopic and spectroscopic techniques. First, interactions between the cell wall and the AuNPs were imaged visually using different microscopic techniques, including confocal laser scanning microscopy (CLSM), AFM, scanning electron microscopy (SEM) and transmission electron microscopy (TEM),and. AFM was used to perform micro-rheological experiments to analyse the physical stiffness of the fungal cell with and without the presence of AuNPs, to determine the impact of the AuNPs on the physical properties of the cell. Synchrotron macro attenuated total reflection–FTIR (macro-ATR-FTIR) measurements were then performed to

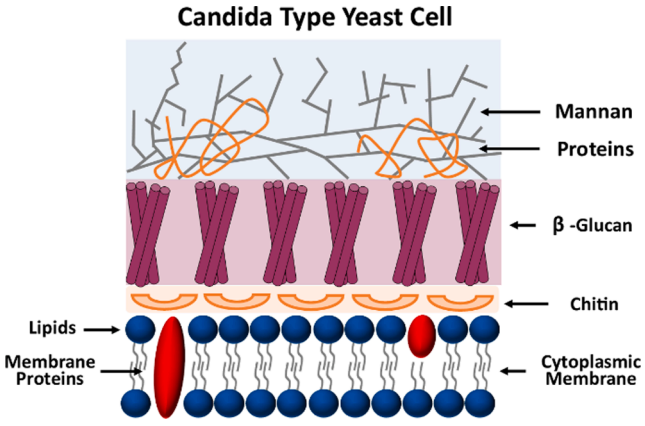

Schematic 1. Illustration of the cell wall and membrane of Candida type yeast cells. Note: the top of the diagram is the outer surface. The schematic is not to scale and is shown for compositional comparison.

obtain information on biochemical changes caused by the nanoparticle interactions. The overall morphology was assessed by CLSM, SEM and TEM. 100 nm AuNPs were selected as the model nanoparticle as they are inert and represent a compromise between nanoparticle size and the imaging resolution provided by analytical technique used in this study. The results obtained from this work provide a new fundamental understanding of the ways in which nanoparticles, and more broadly nanomaterials, interact with fungal cell walls using advanced imaging techniques to reveal changes to live fungal cells after introducing the AuNPs.

2. Materials and methods

2.1. Gold nanoparticles

The nanoparticles used in this project were commercially sourced (Sigma-Aldrich) spherical, citrate-capped AuNPs with a nominal diameter of 100 nm. The particles were stored dispersed in a solution of phosphate buffered saline (PBS) with a concentration of 3.45×10^9 particles per mL. Citrate was employed as the stabilising and capping agent [13].

2.2. Preparation of microbial suspension

C. albicans (18-29511395) was obtained from South Australia Pathology Laboratory. The cells were cultured on potato dextrose (PD) agar plates for two days at 25 °C. *C. albicans* was purposefully cultivated at 25 °C to prevent the yeast cells from undergoing morphogenesis into filamentous cells, which typically occurs at higher temperatures (~37 °C). By maintaining a lower temperature, we ensure study of the yeast form of *C. albicans*, which is relevant for both pathogen-based and environmental investigations and allows for better control over the growth and morphological characteristics of the organism. Importantly, cells were still healthy, grew well on the agar plates (see Figure S1), and were observed to divide in AFM experiments (See Figure S2). Microbial suspensions were created by equilibrating a small number of cells in 2 mL of potato dextrose broth for 1 h before experimentation. This allows cells to homogenize and reach stationary phase prior to experimentation. This concentrated microbial suspension was then diluted down to approximately 6×10^6 cells per mL for experiments. Cellular concentration was determined using a UV/vis detector to measure the optical density of the suspension (Cary 3500 UV–Vis Spectrophotometer, Agilent, Santa Clara, CA 95051, United States).

2.3. Cell immobilisation for AFM

Cells were immobilised for AFM imaging using a polydopamine coated glass cover slip. Polydopamine is positively charged under physiological condition, which allows for the immobilisation of negatively charged microbial cells through physisorption effects [58,82,83]. Previous studies have shown that this method of immobilisation is not cytotoxic [84], and leads to minimal changes to the immobilised cells [11,58]. Immobilisation occurred on a glass coverslip using a modified version of a previously described method [11,85,86]. In short, a solution of dopamine hydrochloride (Sigma Aldrich, 100 %) with a concentration of ~ 8 mg/mL was prepared in PBS. 500 μL of this solution was then added to a 35 mm Flurodish, which fully wet the coverslip surface. The solution was left for 30 min to allow for polymerisation of polydopamine to the coverslip. The surface was then washed with a small volume of PBS three times, after which 100 μL of the prepared microbial cell suspension was added and left to adhere for 1 h. After this time, excess, non-adhered cells were removed by washing with PBS three times. The Flurodish was then half-filled with PBS and these immobilised cells were used for both AFM and CLSM imaging. Treated samples were prepared by adding 100 μL of 100 nm AuNPs in PBS solution (3.45×10^8 particles per mL) to the dish after immobilisation was completed. This provided a ratio of ~ 500 AuNP:1 fungal cell for experimentation, which would allow good cell coverage to monitor AuNP-cell interactions. Particles were allowed to equilibrate with the system for 5 min prior to the AFM scanner being introduced, and then a further 25 min to reach a total of 30 min exposure prior to imaging. It must be noted that the AFM is a live imaging technique, which means that imaging continued past this equilibration time, whereas samples made for electron microscopy and ATR-FTIR were fixed after 30 min of AuNP exposure. This means some differences in time points are unavoidable due to the inherent differences between techniques.

2.4. AFM

AFM images were obtained using a JPK nanowizard 4 (JPK BioAFM Business, Am Studio 2D, 12,489 Berlin, Germany) AFM. Images and force measurements were obtained using ContGD-G cantilevers (BudgetSensors, Innovative Solutions, Bulgaria, nominal spring constant K_c = 0.2 N/m). All cantilevers were tuned using the thermal spectrum method [87]. The JPK instrument was operated in both QI and contact mode for imaging and force measurement, respectively. All measurements were obtained in liquid. Data analysis was completed using a combination of JPKSPM data analysis software package and the Gwydion software package [88].

2.5. CLSM

CLSM images were obtained using a ZEISS LSM 880 Airyscan upright microscope (Oberkochen, Germany). Cells were dyed using Calcofluor White, a cell wall stain which binds to cellulose and chitin, and fluoresces at a 360/430 nm wavelength (Thermo Scientific, 100 %) [89]. AuNPs were found to auto-fluoresce at an emission of ~ 620 nm [90]. Images were obtained using the high-resolution Airyscan mode.

2.6. SEM

Scanning electron micrographs were obtained using FEI Verios Scanning Electron Microscopy (VP, Oberkochen, BW, Germany) at 3 kV using methods previously described [45,91,92]. Cell suspensions were dropcast onto silicon wafers and allowed to equilibrate for 30 min. Samples were then immobilised by chemically fixing both untreated control cells, and cells which had been exposed to 100 nm AuNPs for 30 min using a mixture of 3 % glutaraldehyde (Sigma-Aldrich) and 3 % formaldehyde (Sigma-Aldrich, 95 %) in sodium cacodylate buffer pH 7.4 solution (ProSciTec, QLD, Australia), followed by fixing with 1 % osmium tetroxide (Sigma-Aldrich, 98 %) in Milli-Q water. The fixed samples were then serially dehydrated using ethanol with a concentration of 30 %, then 50 %, 70 %, 90 %, 100 % and finally 100 % again. The dehydrated samples were coated with a thin, 5 nm film of iridium prior to imaging. This methodology allows for retention of cell integrity during the SEM imaging process, and is aligned to protocols previously established [11,32,45,46,93].

2.7. TEM

TEM images were obtained using a JEOL 1010 microscope (JOEL, Musashino, Akishima, Tokyo, Japan) equipped with a Gatan Orius SC1000 CCD camera and operated at an acceleration voltage of 80 keV. For isolated AuNP samples the particles were dehydrated onto a holey carbon TEM grid (300 mesh copper, EMResolutions) from stock solution. For biological samples, the fungal cells were prepared using the methods described above, with and without 100 μL of 100 nm AuNPs to 1 mL of microbial cell solution. After 30 min the treated cells, as well as an untreated control sample were chemically fixed initially using 2 % formaldehyde (diluted from powder paraformaldehyde) and 2.5 % glutaraldehyde in 0.1 M sodium cacodylate buffer pH 7.4 for 30 min, and then post-fixed with 1 % osmium tetroxide and 1.5 % potassium

ferrocyanide (Sigma-Aldrich, 98 %) in Milli-Q water for 1 h. Following fixation, the cells were rinsed thrice in distilled water and centrifuged at 800*g* for 5 min each time. The cells were further dehydrated with increasing gradient of ethanol from 50 % to 100 % ethanol for 15 mins for each step. Following ethanol treatment absolute acetone was added twice to the cells for 30 mins for complete dehydration. After dehydration the cells were infiltrated twice with equal parts of acetone to Spurr's resin (Sigma-Aldrich) (1:1) as described previously [94]. As a final step the cells were infiltrated twice with 100% percent resin under vacuum conditions. Finally, the resin containing cells were incubated at 70 °C for 24 h. Ultrathin sections of 90 nm thickness of the cells were cut with a diamond knife (Diatome, Switzerland) on a UCT ultramicrotome (Leica Ultracut, Germany) and post-stained. These protocols have been developed in house to minimise cellular damage during microtomy and retain cell structure for TEM imaging [46,95,96]. Images were examined using the Gatan Microscopy Suite software version 2.3 (Gatan Inc., Pleasanton, USA) (Gatan, 2013).

2.8. DLS

Dynamic light scattering (DLS) experiments were performed using an ALV-5022F light scattering spectrometer equipped with a laser wavelength of 633 nm. 1 mL of a sample was measured in a cylindrical glass cuvette with an inner diameter of 8 mm (LSI Instruments, Fribourg) held in a scattering vat at room temperature.

2.9. Synchrotron macro ATR-FTIR

Synchrotron macro ATR-FTIR measurements were performed at the Infrared Microspectroscopy (IRM) beamline at the Australian Synchrotron using a Bruker Hyperion 3000 FTIR microscope equipped with a liquid nitrogen-cooled narrow-band mercury cadmium telluride (MCT) detector, coupled to a VERTEX V80v FTIR spectrometer (Bruker Optik GmbH, Ettlingen, Germany). The spatially resolved distribution of chemical functional groups present in clusters of *C. albicans* cells, both with and without 100 nm diameter AuNPs were imaged in ATR-FTIR mapping mode [69,75,97]. An in-house developed macro ATR–FTIR device equipped with a 250 μm diameter facet germanium (Ge) ATR crystal ($n_{Ge} = 4.0$) and a 20 × IR objective (NA = 0.60; Bruker Optik GmbH, Ettlingen, Germany) was used for the chemical imaging experiment [77]. The high refractive index of the Ge ATR crystal coupled with the high numerical aperture (NA) objective used in this device, along with the synchrotron-IR beam, allows for the surface characterisation of microbial biofilms to be performed at high spatial resolutions with a pixel size of less than a micron.

C. Albicans was grown in potato dextrose nutrient broth as outlined in the preparation of microbial suspensions described above. The samples were then centrifuged to form a pellet, which was fixed using 4 % formaldehyde in 0.1 M sodium cacodylate buffer pH 7.4. The samples were then drop-cast onto a silicon wafer and air dried, before being mounted onto an aluminium disc, which was placed onto the sample stage of the macro ATR-FTIR device. The Ge ATR crystal was subsequently brought into the focus of the synchrotron-IR beam and a background spectrum was recorded in air using a 4 cm^{-1} spectral resolution and 256 co-added scans. The sensing facet of the Ge ATR crystal was then brought into contact with the sample and a synchrotron macro ATR-FTIR spectral map was acquired. Each spectrum was collected using a beam defining aperture providing a nominal measurement diameter of 3.13 μm per pixel and 0.5 μm step intervals, 30 × 30 μm scans were taken resulting in a total of 3600 spectra. For each pixel, the synchrotron macro ATR–FTIR spectrum was recorded over a spectral range of 3900–950 cm^{-1} using 4 cm^{-1} spectral resolution and 16 co-added scans. Blackman-Harris 3-Term apodisation, power-spectrum phase correction, and a zero-filling factor of 2 were set as the default acquisition parameters using the OPUS 8.0 software suite (Bruker), which was also used for the initial data analysis.

Prior to analysis, the spectra were smoothed (25 points), the baseline was then corrected using a concave rubber band correction (10 iterations and 64 baseline points), and the spectra were normalized using min–max vector normalization. Chemical maps were generated from the embedded spectra by integrating the area under the relevant peaks using the OPUS 8.0 software. Multivariate data analysis was performed using CytoSpec v. 1.4.02 (Cytospec Inc., Boston, MA, USA) and the Unscrambler X 11.1 software package (CAMO Sofware AS, Oslo, Norway). Two spectral regions covering 3000–2800 cm^{-1} and 1705–1025 cm^{-1} were chosen for further analysis as they are the regions containing the most biological information for microbial samples including the key absorption peaks associated with lipids, proteins, polysaccharides, and nucleic acids [69,71,75].

Hierarchical cluster analysis (HCA) was used as a quality control test. HCA analysis was conducted using Ward's algorithm, and cluster imaging was performed using the processed second derivative spectra by assigning five clusters to be generated. The most suitable HCA clusters were selected for further analysis based on three criteria, including the signal to noise ratio (SNR), the absorption intensity of the amide I band (1705–1600 cm^{-1}), and the number of individual spectra from which the cluster was comprised. Under these criteria, an ideal cluster would have a high SNR (i.e. good spectral quality), a prominent amide I peak, take up a reasonable portion on the chemical map, and have a good correlation with the corresponding visible cell image.

Second derivative spectra were produced using the Savitzky–Golay algorithm with 9 smoothing points and a polynomial order of 3, in order to remove the broad baseline offset and curvature [98]. These second derivative spectra were further processed using the extended multiplicative scatter correction (EMSC), to remove light-scattering artefacts and normalise the spectra accounting for pathlength differences [69,99,100]. After the EMSC correction, principal component analysis (PCA) was performed using The Unscrambler X 10.4 software package (CAMO Software AS., Oslo, Norway).

3. Results and discussion

3.1. Light and electron microscopic investigations

AuNPs where characterised using TEM and DLS as shown in Fig. 1 to confirm their size and morphology. TEM micrographs confirmed an average particle diameter of 99.2 ± 2.4 nm (n = 75), with all measurements displayed as a histogram (Fig. 1B). Selected area electron diffraction (SAED) images of the particles were also obtained (Fig. 1A, inset). The SAED image shows diffraction ring patterns corresponding with those of crystal planes (311), (220), (200), and (111). This is consistent with that of elemental gold with a face centred cubic (FCC) lattice structure, and is the most commonly reported lattice structure [101]. DLS analysis found the average hydrodynamic radius of the AuNPs to be 53 ± 5 nm (Fig. 1C). As such, both the TEM and DLS data are commensurate with ~ 100 nm AuNPs.

Images of whole *C. albicans* were obtained using a combination of in situ and ex situ microscopy techniques, including AFM, SEM, TEM, and CLSM. Images were obtained with and without exposure to 100 nm AuNPs. This allowed investigation into the fungal cell interface as a result of AuNP interactions. Control and treated images are shown in Figs. 2 and 3, respectively. SEM images were obtained to confirm the native structure of the fungal cells of interest, and show that the cells appear ellipsoidal in shape with intact morphology, as is typical of *C. albicans* (Fig. 2) [7,8,79,80,104]. Further, the cells show bud-scaring typical of the species' reproduction cycle (green arrow in Fig. 2A). TEM images of ultrathin sections ~ 90 nm of untreated *C. albicans* were obtained that provided an insight of the cellular ultrastructure (Fig. 2B). In this process, the samples were fixed within a resin prior to ultramicrotomy to produce ultrathin cross-sections, allowing for transmission of electrons through the sample. Fig. 2B shows a *C. albicans* cell dividing, and subcellular structures can be clearly observed, including the cell

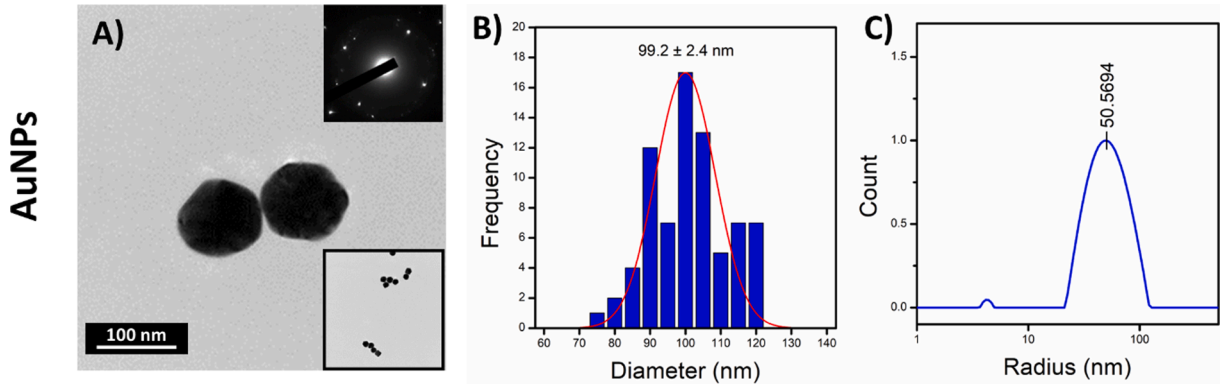

Fig. 1. Characterisation of 100 nm citrate-capped AuNPs. A) TEM images of the AuNPs. The top right shows the SAED image patterns indicative of gold with a face centred cubic (FCC) lattice structure.[102,103] A lower magnification image is also shown (inset, bottom right). B) Distribution of particle diameter obtained using measurements from multiple TEM images (n = 75 particles) showing average particle size of 99.2 ± 2.4 nm in diameter. C) An example of the distribution of particle radius obtained from DLS analysis showing a particle radius of 50.6 nm, a more accurate measurement was obtained by averaging the results of six scans and produced an average radius of 53 ± 5 nm corresponding to a diameter of 106 ± 11 nm.

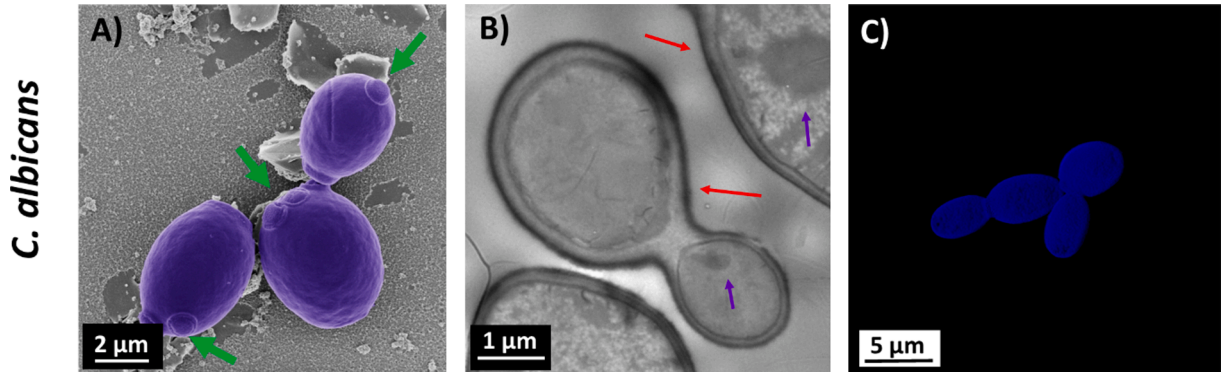

Fig. 2. Characterisation of the *C. albicans* fungal cells. A) False coloured SEM images of whole *C. albicans* cells. Budding scars are visible on all cells (green arrows). **B)** TEM cross-sectional images of *C. albicans* cells in which cellular components including the cell wall (red arrows) and organelles (purple arrows) are visible. **C)** CLSM images showing clusters of whole cells fluorescing blue at 430 nm. Additional control data is shown in Figure S3.

wall (~100 nm thick, red arrows) and organelles (purple arrows). Confocal imaging was also employed to image the cells in situ, which entailed staining the cell wall with calcofluor white, which binds to cellulose and chitin in the cell wall and fluoresces at 430 nm (appearing blue in the images). A representative super-resolution CLSM image is shown in Fig. 2C. This data acts as a baseline for comparison of cell viability, where the cells are healthy and functioning as expected.

Following assessment of the untreated cells, similar images were obtained of *C. albicans* cells following exposure to 100 nm AuNPs. This allowed assessment of any physical or structural changes to cells caused by cell-nanoparticle interactions. SEM images were collected and false coloured to differentiate the particles more easily from the cells. The *C. albicans* cells are coloured purple while the AuNPs are coloured red. Fig. 3A shows an SEM image of a cell with nanoparticles adhered to the cell wall surface, but there is no indication of change or damage to the cells due to the AuNPs. Budding scars are also observed in the treated samples, commensurate with control samples (*c.f.* Fig. 2A and Fig. 3A, green arrows).

The cross-sectional TEM images of *C. albicans* cells in Fig. 3B, D-F allow the interior of the cells to be imaged. Importantly, these images do not indicate any cell damage, and other than the presence of the AuNPs, are also comparable to the control images in Fig. 2B. The cell wall is indicated by the red arrow and organelles including the nucleus and chromatin are indicated by purple arrows. Yellow arrows in Fig. 3B indicate the presence of AuNPs. These nanoparticles were observed on the surface of the outer cell wall (Fig. 3D), and within the internal compartment of the cell (Fig. 3F). Close analysis of Fig. 3E reveals a AuNP trapped in the mannoprotein layer (on the cell membrane layer). While occurrences like this were somewhat rare, this shows that the AuNPs can sometimes traverse the cell wall and cell membrane.

Fig. 3C shows CLSM images of clusters of *C. albicans* cells with AuNPs attached to the cell surface, obtained in the same manner as control samples (Fig. 2C). The AuNPs were found to exhibit autofluorescence at ~ 620 nm (red) without the use of a dye, as previously reported in the literature [90]. Fig. 3C shows a 5 µm × 5 µm scanned area in which several AuNPs can be seen attached to the surface of the cell. Figure S3C shows a larger image of a cluster of four cells joined together, where a particle can be seen on the third cell.

In all micrographs, there were no obvious morphological differences or damage to the cell structure between the control and treated samples, which would be expected if the nanomaterials were chemically or physically disruptive to this organism [5,32,45,46,105–108]. The AuNPs antimicrobial activity typically relies on one of two different mechanisms. First is the physical interactions in which the structure of the particle itself disrupts and damages the cell. This mechanism is typical of NPs relying on unusual or sharp shapes including high-aspect ratio gold nanostars [109], gold nanocrosses [110], and gold nanospikes [92]. Alternatively, NPs which would otherwise not possess antimicrobial activity can be functionalised with antimicrobial compounds or materials [111–113]. Together, these data highlight two important pieces of information 1) conventional light-based or electron microscopy cannot discern subtle bio-interfacial, biophysical, or biochemical changes to fungal cells as a function of nanoparticle interactions, and 2) that the spherical, citrate-capped AuNPs do not appear to drastically

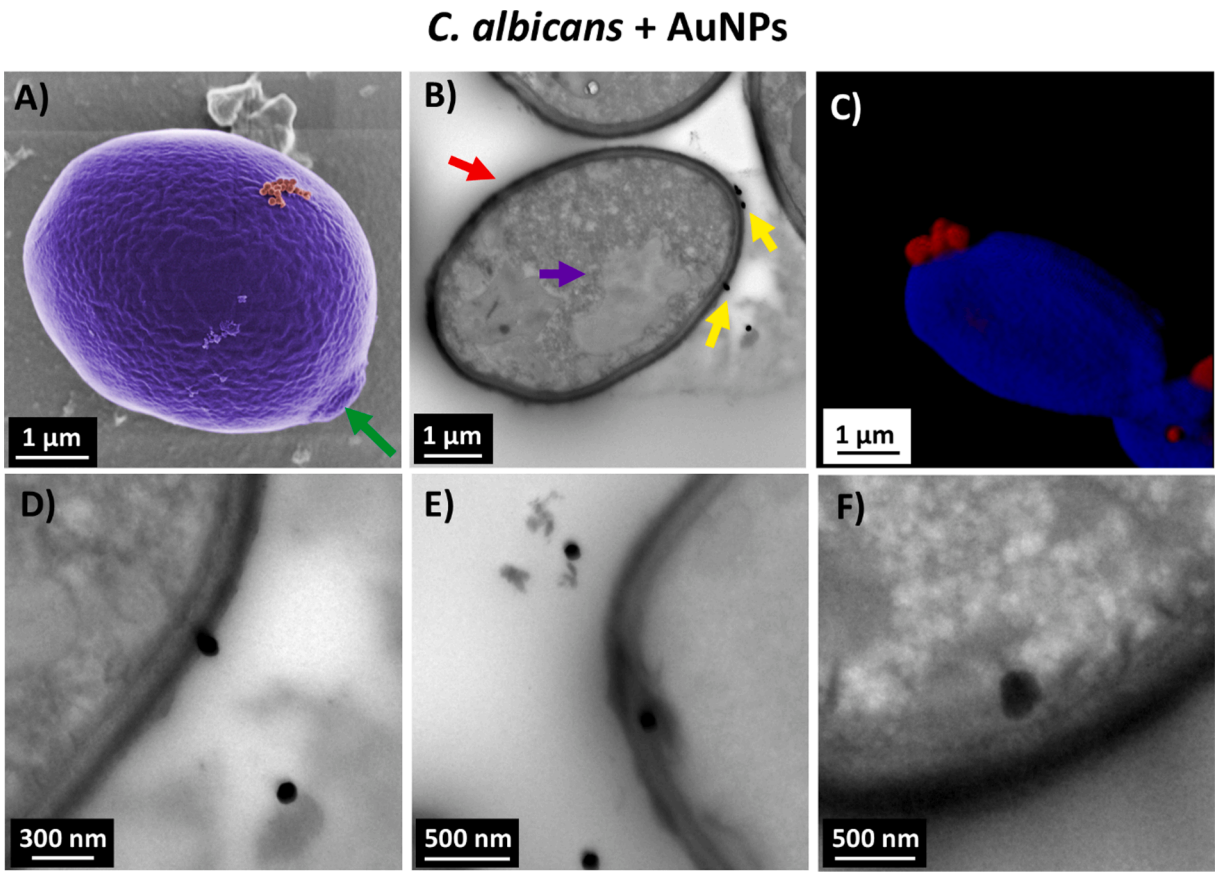

Fig. 3. Characterisation of *C. albicans* cells exposed to 100 nm AuNPs A) False coloured SEM image of whole cells (purple) with nanoparticles (red) visibly clustered on cell surface. A budding scar is highlighted by the green arrow. **B)** Comparatively low-resolution TEM image of whole cells following interaction with AuNPs. The cell wall is clearly visible (red arrow), as are organelles (purple arrow). Some AuNPs are highlighted with yellow arrows. **C)** CLSM images of whole cell wall fluorescing at 430 nm (blue) as a result of calcofluor membrane dye with nanoparticles (red at 620 nm as a result of autofluorescence) visible on the cell surface and in surrounding solution. **D) - F)** Higher-resolution TEM images showing different ways in which nanoparticles interacted with cells. Nanoparticles can be seen attached to the outside of the cell wall (D), passing through a cell wall (E), and inside the cell (F). Additional SEM, TEM, and CLSM data are shown in Figure S4 for this system.

alter the cell interface or cause lethal damage to the fungi [1]. This was confirmed by comparison of fungal growth in control vs. treated systems, which revealed no meaning full difference in fungal viability (see Figure S1). To this end, alternative microscopic techniques were employed to assess the biophysical and biochemical impact of AuNP exposure.

3.2. Atomic force microscopy

AFM was used to obtain morphological bio-interfacial images and nanomechanical data. First, QI mode [114] was employed to obtain high-resolution, in situ images of the *C. albicans* cells, with and without exposure to the 100 nm citrate-capped AuNPs (Fig. 4). In QI mode, the AFM cantilever is rastered across the surface in intermittent contact with the sample, and an individual force curve is obtained at every discrete surface location (a pixel). Images are produced via estimating the point of tip-sample contact for each pixel. Fig. 4A and 4B show the treated and untreated cells, respectively. The cells appear similar to images observed using traditional microscopy (see Figs. 2 and 3). Fig. 4C and 4D show higher-resolution images of the cell wall for the regions denoted by the black boxes in Fig. 4A and 4B. Fig. 4C shows distinct, nanoscale corrugations (or grooves) across the cell wall. This is typical of cell-wall structures of fungi, whereby β-glucan and chitin form a meshed, supportive cell wall structure [9]. These nanoscale features could not be readily observed using electron or light-based microscopy (see Figs. 2 and 3). However, for the treated cells (Fig. 4D), the cell wall of the *C. albicans* appeared flatter and smoother, and small, depressed regions are noted on the cell wall. Comparison of the AFM images with and without AuNPs (Fig. 4A and 4B) reveals that the cells appear to be healthy and are shaped as expected for this species [115–117], meaning that the AuNPs are not causing lethal damage to the fungi. As such, the properties of the cell wall were further investigated using microrheological protocols [118–122] to calculate the Young's modulus of the *C. albicans* cell with and without nanoparticle exposure.

Data was obtained in four steps as shown in Fig. 4E and Fig. 5, including 1) the cantilever was lowered onto the cell surface, 2) A constant force is applied between the cell and the cantilever and held until changes in the tip-cell separation (compression) were no longer noted, 3) the cantilever tip is then modulated at a set frequency and amplitude, and the cantilever response is monitored, 4) The cantilever is then retracted away from the surface (withdrawn). An example of the resulting force profiles as a function of time is shown in Fig. 4E. This measurement can then be related to sample stiffness. A detailed explanation of the mathematics underpinning this calculation of stiffness is shown in the SI and data analysis was based on the work of Alcaraz, Buscemi, Grabulosa, Trepat, Fabry, Farré and Navajas [123]. A histogram showing the comparative stiffness of treated and untreated cells can be seen in Fig. 4F. The primary peak for the treated cells is at a higher Young's modulus value than that of the control sample (330 kPa compared to 75 kPa); however, the smaller secondary peak of the treated sample largely overlaps with the main control peak (100 vs 75 kPa). The Young's moduli of the treated cells appear over a wider range

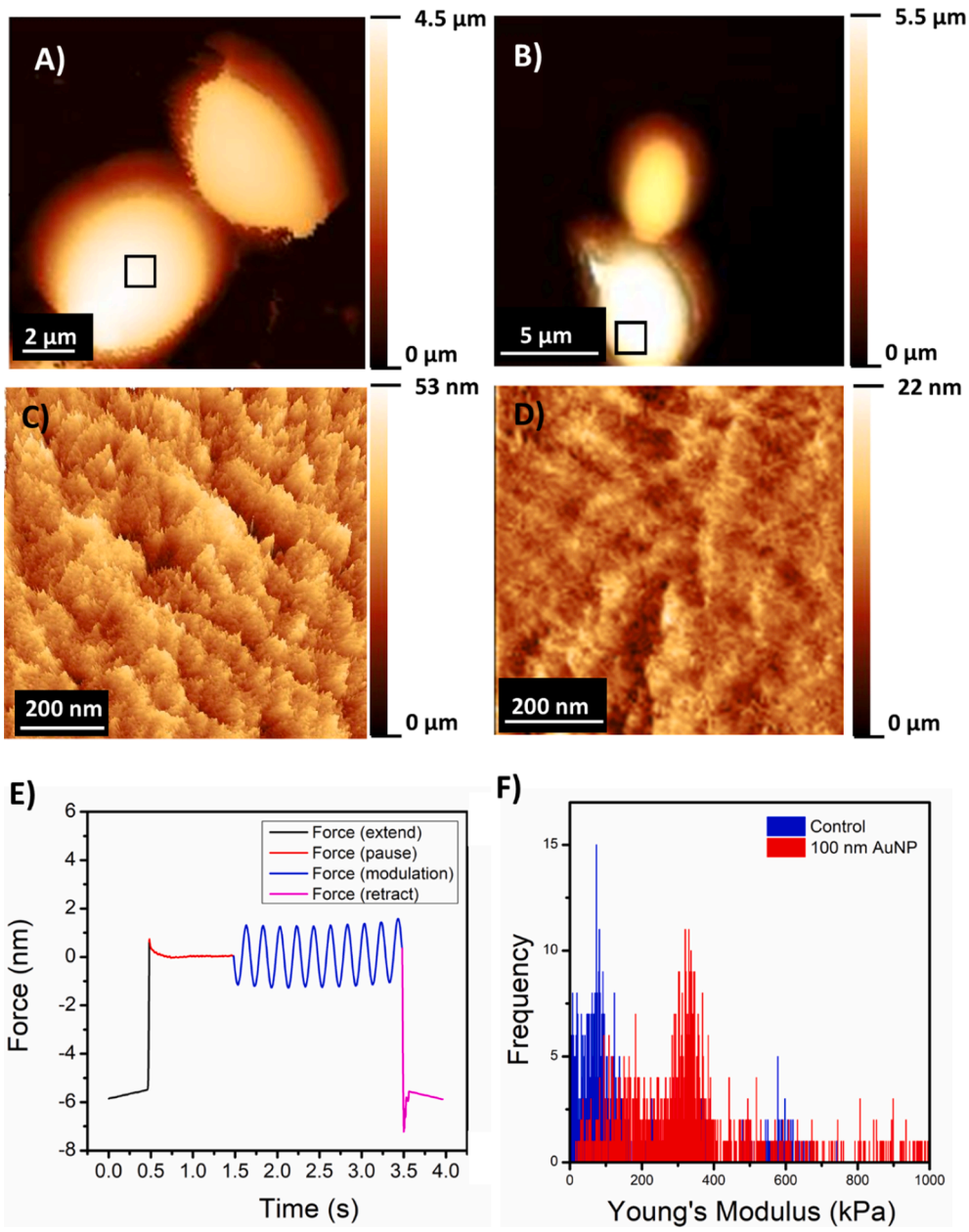

Fig. 4. AFM data of both treated and untreated *C. albicans* cells. A) AFM image of two untreated control cells. **B)** AFM image of two cells treated with 100 nm AuNPs**. C)** Higher resolution image of the cell wall for the area indicated by the black box in A). **D)** Higher resolution image of the cell wall for the area indicated by the black box in B). **E)** A representative single force curve showing four data sections, the approach of the cantilever (black), the cantilever pausing to allow the system to re-equilibrate (red), the modulation section where actual measurements occur (blue), and the retraction of the cantilever (purple) **F)** Frequency histogram of Young's modulus for control cells (blue) and cells treated with 100 nm AuNPs (red) (n = 512 from 8 repeats).

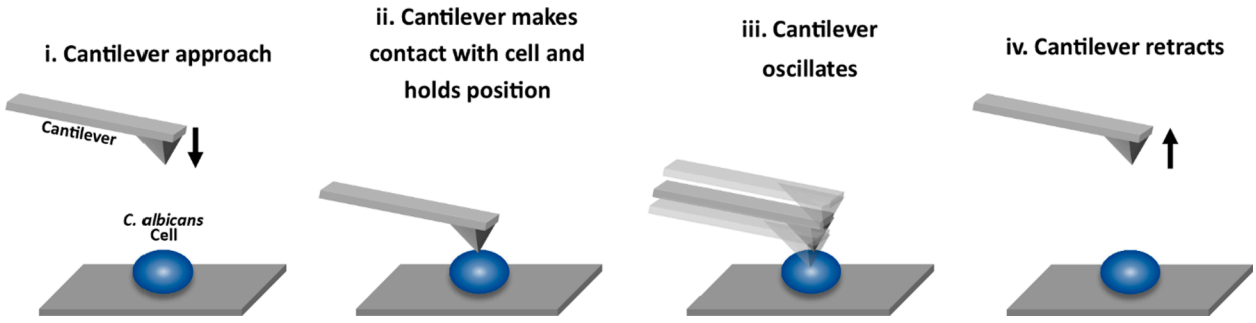

Fig. 5. Schematic showing the method used to obtain stiffness measurements.

of values than do the control cells, indicating localised regions of increased stiffness. This is not surprising given the localised nature of nanoparticle adsorption observed in the electron and light-based microscopy (see Fig. 3). The increase of Young's modulus observed in the treated cells is indicative of an increase in the overall stiffness of the cell. This rigidity could be the result of chemical changes to the cell wall and membrane make-up caused by interactions with the nanoparticles, or it could simply be the result of minor deformations caused by the mass and adhesion of the nanoparticles causing lipids in the membrane to pack more closely together. In fact, AFM has been increasingly used for investigating the stiffness of fungal cells [69,124,125], and their biophysical response to external stimuli [126–129].

3.3. Synchrotron macro ATR-FTIR microspectroscopy

Biochemical changes to the fungal-cell interface as a function of particle interactions were assessed using synchrotron macro ATR-FTIR microspectroscopy. Spatially specific information on the chemical composition of the cells was analysed to observe changes in biochemical makeup of the cells caused by the presence of AuNPs. The key characteristic absorption peaks include methyl/methylene groups (3000–2800 cm^{-1}) for lipids, amide I region (1705–1600 cm^{-1}) for proteins, and the low-wavenumber region (1200–1000 cm^{-1}) for polysaccharides and nucleic acids [75,130]. Representative spectra for the control and treated samples are shown in Fig. 6 (top and bottom, left respectively). Spectra are shown over the spectral window of 3000–1000 cm^{-1}, as previous synchrotron macro ATR-FTIR studies of yeast cells have shown that the major spectral features can be captures within the region [131]. Small differences can be observed between systems, which can be attributed to subtle changes to the major classes of biomolecules within the fungal cells as a function of nanoparticle exposure. Synchrotron ATR-FTIR spatio-chemical maps for both systems, which were produced by integrating the areas under the key characteristic bands mentioned above, are displayed in Fig. 6. The maps represent the distribution of lipids, proteins and polysaccharides observed for the untreated control cells (top) and those after the exposure to the AuNPs (bottom). Strong intensities of ν(C—H) stretching modes of methyl/methylene groups (for lipids) and the amide I band (for proteins) are indicative of the presence of whole cells [132,133], and cell-shaped entities can be seen in the spectral maps, especially in the amide I band region (see Fig. 6, white dashed circles). Assessment of the lipid and Amide I spectral maps (see Fig. 6) shows that a cluster of cells are sampled during the measurement, with greater than 10 fungal cells visible in the spectral maps.

Fungal cell envelopes are typically characterized by a rich composition of glycoproteins, carbohydrates, hydrophobins, and lipids [7,10,12,134]. Additionally, they contain various interstitial extracellular compounds, including monosaccharides, polysaccharides, glucans, proteins, lipids, nucleic acids, melanin, polyols, and hydrophobins [135–137]. These compounds play a vital role in facilitating and promoting fungal surface attachment [138]. The spectral maps show the differences in the chemical composition of the systems investigated, although inspection by eye of these maps does not show distinct difference. Further, the polysaccharide (or carbohydrate) spectral-region maps (see Fig. 6, right) are noisy and devoid of structure. This is due to two reasons: 1) Carbohydrates are the most abundant molecule in the *C. albicans* outer layer of the cell wall, and 2) the extracellular polymeric substances (EPS) of *C. albicans* are polysaccharide rich. Together, this means that the bio-interface is enriched with polysaccharides/carbohydrates, which provides a strong signal almost everywhere at the bio-interface, and results in the maps observed over this spectral region in Fig. 6.

The data was statistically assessed to evaluate major differences between the data sets. The 2nd derivative of each spectra was calculated, and used to assess the overall rate of change of peaks within the spectra, highlighting regions of interest where significant spectral signal is observed. After that, HCA was applied to group spectra into separate clusters based on the degree of similarity. The best cluster group that contained the majority of the key biochemical information of the cells was then selected from each of the two cell types (i.e. control and AuNP-treated groups) based on the three criteria mentioned in Materials and Methods for comparison purposes [24,52,53]. In essence, the HCA approach was used to ensure that high-quality spectra that genuinely contained the key biochemical information were selected as representatives from each cell group, providing a high reliability in discriminating biochemical compositions between control and exposed cells. As an example, Figure S5 demonstrates the HCA results obtained based on

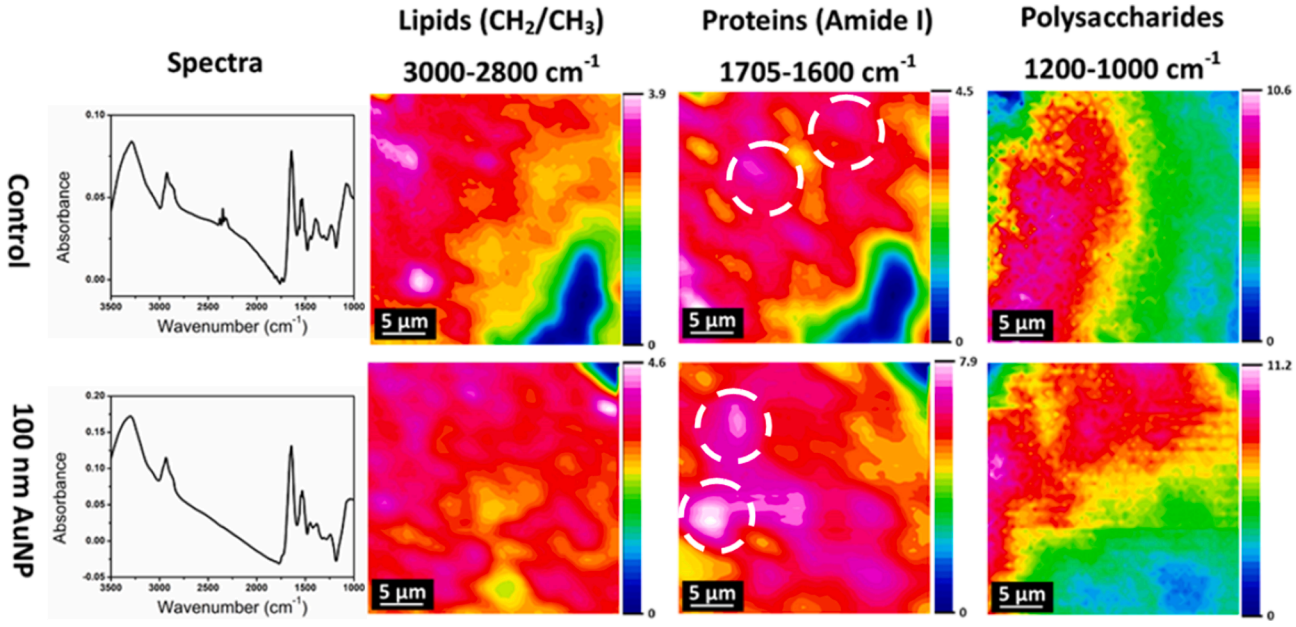

Fig. 6. Comparison of representative synchrotron macro ATR-FTIR spectra (left) and their corresponding high-resolution false-colour maps that represent the distribution of lipids (methyl/methylene), proteins (amide I) and polysaccharides, observed for control *C. albicans* cells (top) and cells after treatment with 100 nm AuNPs (bottom). White dashed circles have been overlaid to draw the eye to the cells. Each pixel is representative of a single spectrum with 3600 spectra composing each image.

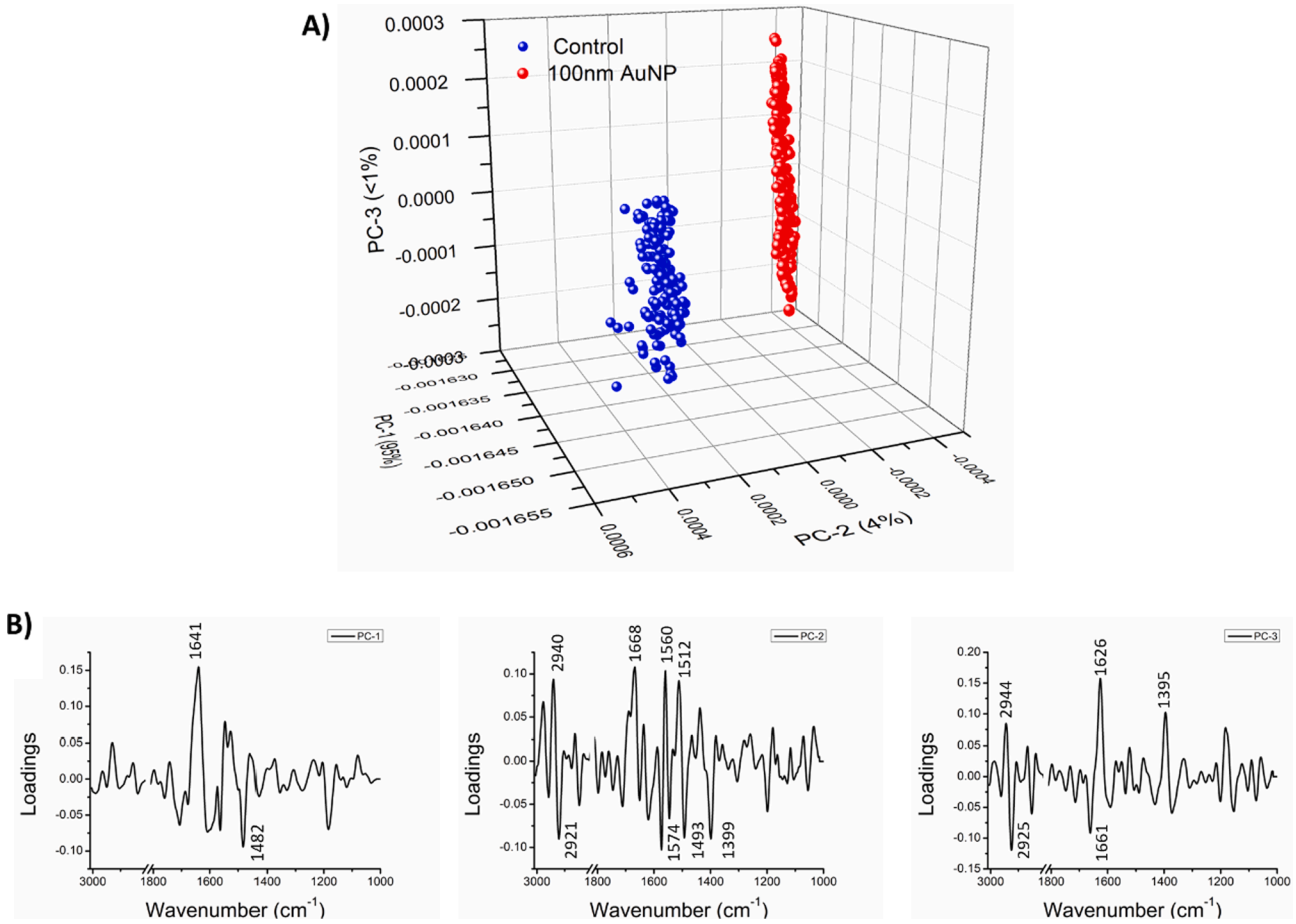

Fig. 7. PCA result showing differences in biochemical compositions between control (blue) and AuNP-treated (red) samples. A) 3D scores plot **B)** Corresponding PC1, PC2 and PC3 loading plots with strong loaded peaks identified and labelled (see Table 1).

the synchrotron macro ATR-FTIR maps of control and AuNP-treated cells. Based on the criteria mentioned above, the grey and aqua clusters were selected as representative groups for the control and AuNP-treated samples, respectively.

PCA was conducted on the chosen spectral cluster to identify distinct changes in the spectra between the treated and untreated systems [54]. In principle, PCA is a statistical technique used to reduce the dimensionality of a dataset while preserving the most important information. When applied to FTIR spectra, PCA identifies the main spectral variations and represents them as a set of orthogonal components, allowing for a simplified interpretation and visualization of the data. This specific statistical approach calculates linear combinations of variables, which best explain the data [139]. In this study, the 2nd derivative spectra were processed using extended multiplicative signal correction (EMSC) models prior to PCA [24,55].

The PCA results, including 3D scores plot and the corresponding PC1,

Table 1
Band assignment of the key influential peaks observed in PC1, PC2, and PC3 loading plots [131].

Wavenumber (cm^{-1})	Assignment
PC1	
1482	$\delta_{scissor}(CH_2)$ from methylene (—CH_2) groups in acyl chains of lipid bilayers in orthorhombic packing
1641	Amide I: antiparallel β-sheet
PC2	
1399	$\delta_s(CH_3)$ and $\delta_s(CH_2)$ of lipids and proteins
1493	ν(C═C) of phenyl rings from the aromatic amino acid phenylalanine (Phe)
1512	Amide II: parallel mode of the α-helix
1560	Amide II: perpendicular modes of the α-helix and antiparallel β-sheet
1574	Adenine (C═N) or unspecified amide II
1668	Amide I: β-turn
2921	ν_{as}(C—H) from methylene (—CH_2) groups of lipids
2940	ν_{as}(C—H) from methyl (—CH_3) groups of lipids
PC3	
1395	$\delta_s(CH_3)$ and $\delta_s(CH_2)$ of lipids and proteins
1626	Amide I: antiparallel β-sheet
1661	Amide I and ν(C═C)*cis*, lipids, fatty acids
2925	ν_{as}(C—H) from methylene (—CH_2) groups of lipids
2944	ν_{as}(C—H) from methyl (—CH_3) groups of lipids

Note: ν_{as} = asymmetric stretch; ν_s = symmetric stretch; δ_s = symmetric in-plane deformation (bend); δ_{as} = asymmetric in-plane deformation (bend).

PC2 and PC3 loading plots, are shown in Fig. 7A and 7B, respectively. The key spectral regions used for evaluating the variation between treated and untreated samples remain those associated with lipids (methyl/methylene stretching region), proteins (amide I region), and structural polysaccharides. The PCA approach allows for statistical identification of significant difference between the control and treated datasets. In this case, the first two PCs were found to capture the majority of statistical variance within the systems (99 % overall variability). While PC1 and PC2 represent major and minor differences between the two cell groups (95 % and 4 % respectively), PC3 possesses the information on the cellular variations within individual groups (<1 %) [132].

PCA loading plots (Fig. 7B) were used to identify which wavenumbers were significantly different between the treated and untreated fungal cells. Peaks which had a loading greater than 0.08 (or less than −0.08) where considered significant and are given in Table 1. The wavenumber of these peaks was assigned to specific functional groups based on past literature and as described in Table 1.

As described above, PC1 accounted for 95 % of the difference between the treated and untreated samples. Therefore, the strong loaded peaks at 1641 and 1482 cm^{-1} suggests that biochemical differences between the two groups were primarily in the cellular protein and acyl chains in lipid bilayers, respectively. The PC2 loading plot, on the other hand, reveals strong influential peaks associated with C—H stretching and bending modes of methyl/methylene groups of lipids (2940/2921 and 1399 cm^{-1}) and amide I/II bands of proteins (1668, 1574, 1560, 1512 and 1493 cm^{-1}). The PC3 loading plot provides additional information on the chemical variations within the groups, which also point to the methyl/methylene groups of lipids (2944/2925 and 1395 cm^{-1}) and amide I protein structures (1626 and 1661 cm^{-1}). Accordingly, the overall PCA results suggest that most biochemical differences occurred in the lipid and protein components of the cells, which are likely associated with the fungal cell wall or membrane, in agreement with the microscopy results discussed above. It must be noted that cells were fixed in 4 % formaldehyde (0.1 M sodium cacodylate buffer, pH 7.4) prior to synchrotron macro ATR-FTIR. The sample was rinsed thoroughly, however, the C═O bond may contribute to the obtained spectra; however, this addition to the spectra signal would be consistent between control and treated samples, meaning that changes are the result of Fungi – AuNP interactions. Our previous work has developed this fixation approach [46,75,77,93,131,140], which is commensurate with other literature in the field [74,141]. The use of fixative is to preserve samples during the drying process, which is necessary to obtain high-quality ATR-FTIR spectra.

A combination of electron microscopy, AFM, synchrotron ATR-FTIR microspectroscopy, and statistical data analysis techniques have shown AuNPs can cause distinct morphological, bio-mechanical, and biochemical changes to a model fungal cell, *C. albicans*. Together, these techniques show that AuNPs behaved in three specific ways: 1) cell wall adsorption/adhesion, 2) cell membrane distortion, and 3) cellular uptake. Additionally, AFM imaging and nanomechanical measurements showed that the presence of the AuNPs led to a smoothing of the biomembrane and a significant impact on the stiffness of the cell (see Fig. 4). Young's Modulus measurements for the AuNP treated samples showed a bi-modal profile (see Fig. 4), which may result from uneven NP adsorption across the cell interface, as observed in the microscopic images (see Fig. 3). The synchrotron ATR-FTIR results showed subtle changes to the biochemistry of the proteins and lipids within the fungal cells when exposed to AuNPs, which are likely related to changes in cell morphology and stiffness. While we did not observe nanoparticle aggregation in AFM or confocal experiments, it is possible that some aggregation occurred. We expect that aggregates would interact differently with the cell interface and would be less likely to diffuse into the cell interior.

Fungal surfaces, cell wall, membranes, and its internal organisation are complex entities, and predictive models of nanomaterial-fungi interactions, which can predict toxicity or biocompatibility, are yet to be developed [1,3,4,19]. In this vein, biophysical studies, including those presented here, are important to better understand the interactions between nanomaterials and fungal cells. To date, studies have investigated the antifungal behaviour of metal [33,47,49,50,142–144] and organic [145] NPs towards fungal cells [5,23,47]. Meanwhile, a large portion of literature have described the bio-synthesis of a variety of metal nanoparticles from fungal cells [63,68,146,147]. Together, these studies indirectly highlight the importance of nanoparticle-fungi interactions for a wide variety of nanoparticle sizes, geometries, and surface chemistries, while not directly examining the fundamental behaviour of NPs at the fungal cell interface. This means that the biophysical investigations of NP-fungi interactions have been largely understudied.

For bacterial and fungal systems, metal-based nanoparticles are often purported to be excellent antimicrobial candidates [2,5,23,32,45,47,50,105,148,149], as well as potential biofilm disruptors [107,108,150–154]. The mode of antimicrobial action can arise from two main aspects: 1) chemical and 2) physical interactions. Chemically, antimicrobial nanoparticles can disrupt microbial membranes and interfere with vital cellular processes, via either metal ions or the generation of reactive oxygen species (ROS). Metal ions, once released, can bind to essential biomolecules, disrupting enzymatic reactions, and altering microbial metabolism, while ROS can cause oxidative stress, all of which lead to microbial cell damage [23]. Moreover, the release of metal ions can initiate destabilization of the microbial cell wall, compromising structural integrity. Physically, the small size and high surface area of metal nanoparticles enable them to disrupt the microbial cell wall or penetrate the microbial cells, all of which can damage DNA, proteins, and lipid structures. Overall, the dual action of antimicrobial metal nanoparticles, combining both chemical and physical effects, underscores their potential as effective agents in combating various pathogens and antimicrobial-resistant strains. Importantly, the magnitude of these effects is dependent on the size [138,140] and chemistry [141] of the nanoparticle, while the effect of the shape of the particle is less well known [23]. For instance, the most prevalent example of antimicrobial nanoparticles is silver, which release silver ions and interact with cell membranes, nucleic acids and the thiol and amino groups which are present in proteins, with bactericidal [67,74,126] and fungicidal [127] effects. Other metals, such as copper, also elicit antimicrobial action via similar pathways, although microbes are capable of evading this mechanism under certain conditions [47]. In contrast, the treatment of established biofilms with nanoparticles is often not achieved, as the biofilm itself forms a protective barrier which is poorly penetrable by antimicrobials and often only microbes at the biofilm surface are killed by antimicrobial treatment, while bacteria residing in deeper layers of a biofilm survive [23].

The citrate-capped 100 nm AuNPs were specifically chosen for this study, as they are largely inert, do not leach metal ions, and allow for only biophysical interactions to be investigated at the *C. albicans* interface. This allows the study to decouple chemical effects, such as ion interactions, which would be expected in Ag and Cu nanoparticle systems [32,33,48,50,155–160]. Importantly, the biophysical response observed in our system could be similar for other fungi and bacteria systems, however, would likely subtley vary as a function of pathogen, as well as nanoparticle size, chemistry, and geometry. For instance, the cell wall and physiology of a microbe, or cell in general, would be expected to alter the precise nanoparticle-cell interaction, and the type of nanoparticle will ultimately dictate specific interaction [5]. Moreover, microbial biofilms are more robust biological constructs, which will most likely affect the degree of biophysical response at the cell-nanoparticle interface [7,75,81,93,136,161–164]. The breadth of these investigations is beyond the scope of this study, but it is something that should be considered by research groups in the future.

The biophysical response and nanomechanical alteration of mammalian [165–169] and bacterial cells [5,11,23,45,46,105,108,170] as a function of nanoparticle, and more broadly nanomaterial, exposure

has been more widely studied. In general, studies have shown that intra- and extra-cellular NP-cell interactions can alter cell physiology [171], modulate the cell stiffness [167], affect cellular migration [165], and induce cell death [5,23,172–177]. Review of this vast literature highlights that many factors influence the bio-functionality of nanoparticles, and in-turn their cellular interactions, including: nanoparticle size, morphology, geometry, surface charge, materials chemistry, surface composition (and/or functionalization), capping agent chemistry [169], and the presence of bio/protein corona [178,179]. Interactions are also influenced by the chemical and physical properties of the cells, including size, charge, membrane permeability, and extra-cellular appendages [6,180]. The majority of academic [1,4,10] and medical studies [181] in the area of mammalian cells have investigated living systems via non-specific bio-assays, which provide limited information about the biophysical response of nanomaterial-cell interactions [182–185], meaning that finer biochemical and structural alterations are not probed. Rasel *et al.* [167,186] have shown distinct increases in mammalian cell stiffness after nanoparticle exposure and subsequent uptake, which is in good agreement with the AFM data obtained in this study. It must be noted that living systems are complex, and while these factors contribute to our understanding of nanoparticle-cellular uptake, the field is still evolving, and further research is needed to fully comprehend the complexity of this process. Indeed, for fungal systems nanomaterial-induced changes in the cell stiffness, physicochemical, and adhesive properties have not been reported [14-16].

The above-mentioned complexity of the systems has led people to investigate model cell walls and/or membranes along with metabolic pathways. Often lipid bilayers or liposome systems [61,182,187–189], with varying complexity, are used as cell membrane mimics to investigate nanoscale interactions, such studies have begun to elucidate the underlying processes and dynamics of nanoparticle adsorption [12], desorption [8], translocation [28], and internalization/uptake [9,29,13] in nanomaterial-lipid systems at the molecular level. Several experimental [13,190–193] and computational studies [194–202] have shown the interactions of AuNPs with these model membranes, highlighting the importance of the particle composition, ligand-cap dynamics, and the underlying membrane composition. Importantly, the AuNP adsorption and membrane inclusion can disrupt the mechanical stability and normal ordering of a lipid bilayer [179,190–196], which is consistent with the results shown here for the biophysical and chemical response of *C. albicans* to 100 nm citrate-capped AuNPs, albeit for a much simpler system. We believe that this study will better highlight the importance of biophysical studies of nanomaterial-fungi interactions, as well as provide new directions for further studies in this field of research. It should be noted that this type of study does not provide molecular-scale insight, but rather information on the global changes of the fungal cells with the addition of nanoparticles. The AFM- and macro FTIR-based techniques used here are largely limited to interfacial investigation, and cannot easily report on intracellular phenomena. As such, we suggest that further analytical techniques and molecular dynamics simulations could be used in the future to further our understanding of these systems.

4. Conclusion

In summary, the interactions taking place between citrate-capped 100 nm AuNPs and *C. albicans* fungal cells were assessed using multimodal imaging and advanced analytical methods. First, microscopic images of both treated and control cells were obtained using CLSM, AFM, SEM and TEM. Following this, AFM was used to investigate morphological and nanomechanical changes to the *C. albicans* cells as a result of nanoparticle interactions. In addition, advanced synchrotron macro ATR-FTIR microspectroscopy was used to gain insights into biochemical changes resulting from cell-nanoparticle interactions.

The imaging techniques identified the presence of nanoparticles adhered to the surface of the cell wall in most cases, and occasionally crossing the cell wall and entering the intracellular cavity. Microrheological experiments revealed an increase in the Young's modulus of the cell, indicative of an increase in stiffness following AuNP exposure. In particular, the data from the synchrotron macro ATR-FTIR analysis showed significant changes to the biochemical compositions between the control and exposed cells, which were primarily attributed to changes to the phospholipids and proteins in the cell well and cell membrane. Overall, these investigations into the physical and biochemical changes of fungal cells as a result of interactions with nanoparticles provide insights into fungal cell-particle interactions, which may influence many different areas of nanomedicine including drug delivery, disease detection and diagnostics, and cellular imaging.

In the future, we believe the techniques combined in this work could be utilized to bridge qualitative and quantitative assessments of not only nanoparticle-fungal interactions, but also more broadly the biophysical interactions of organic and inorganic materials with living and model biological entities. For example, the biophysical interactions of biomolecules [203–205], proteins [206–208], toxins [209–211], antiseptics [212], and therapeutics [213–215], as well as organic, inorganic, and soft matter nanoparticles [1,3,4,19,74,77,216]. In the area of nanoparticles, a wide variety of nanoparticle sizes, geometries, and surface chemistries could be explored at bio-interfaces to better elucidate structure–function relationships [19,61,169,171,189,199,217,218]. Moreover, the effect of nanoparticle concentration on fungal cells, and more generally biological entities, should be studied, as there will likely be concentration-dependent effects. We believe our work highlights the importance of assessing biophysical changes at the nanomaterial-fungi interface, and more broadly the effect of nanoparticle interactions at bio-interfaces. This type of study will provide new directions for further studies in this field of research.

CRediT authorship contribution statement

Rowan Penman: Methodology, Validation, Formal analysis, Investigation, Data curation, Writing – original draft, Writing – review & editing. **Rashad Kariuki:** Methodology, Validation, Formal analysis, Investigation, Data curation, Writing – original draft, Writing – review & editing. **Z.L. Shaw:** Methodology, Validation, Formal analysis, Investigation, Data curation, Writing – original draft, Writing – review & editing. **Chaitali Dekiwadia:** Methodology, Validation, Investigation, Data curation, Writing – review & editing. **Andrew J. Christofferson:** Methodology, Validation, Investigation, Data curation, Writing – review & editing. **Gary Bryant:** Methodology, Validation, Investigation, Data curation, Writing – review & editing. **Jitraporn Vongsvivut:** Methodology, Validation, Investigation, Data curation, Writing – review & editing. **Saffron J. Bryant:** Conceptualization, Methodology, Validation, Formal analysis, Investigation, Resources, Data curation, Writing – original draft, Writing – review & editing, Supervision, Project administration, Funding acquisition. **Aaron Elbourne:** Conceptualization, Methodology, Validation, Formal analysis, Investigation, Resources, Data curation, Writing – original draft, Writing – review & editing, Supervision, Project administration, Funding acquisition.

Declaration of Competing Interest

The authors declare that they have no known competing financial interests or personal relationships that could have appeared to influence the work reported in this paper.

Data availability

Data will be made available on request.

Acknowledgements

Z.L.S. acknowledges this research was supported by an AINSE Ltd. Postgraduate Research Award (PGRA: ALNSTU13134). A.E. is supported

by an Australian Research Council (ARC) Discovery Early Career Research Award (DECRA) (DE220100511). The authors would like to acknowledge and thank both the Microscopy and Microanalysis Facility (RMMF) and the MicroNano Research Facility (MNRF) at RMIT University for the use of their facilities and the expertise of their staff.

Appendix A. Supplementary material

Supplementary data to this article can be found online at https://doi.org/10.1016/j.jcis.2023.10.017.

References

[1] H. Bahadar, F. Maqbool, K. Niaz, M. Abdollahi, Toxicity of nanoparticles and an overview of current experimental models, Iran. Biomed. J. 20 (1) (2016) 1–11.
[2] T. Patil, R. Gambhir, A. Vibhute, A.P. Tiwari, Gold Nanoparticles: Synthesis Methods, Functionalization and Biological Applications, J. Clust. Sci. (2022).
[3] S. Mashaghi, T. Jadidi, G. Koenderink, A. Mashaghi, Lipid Nanotechnology, Int. J. Mol. Sci. 14 (2) (2013) 4242–4282.
[4] C. Contini, M. Schneemilch, S. Gaisford, N. Quirke, Nanoparticle-membrane interactions, J. Exp. Nanosci. 13 (1) (2018) 62–81.
[5] Z.L. Shaw, S. Kuriakose, S. Cheeseman, M.D. Dickey, J. Genzer, A. J. Christofferson, R.J. Crawford, C.F. McConville, J. Chapman, V.K. Truong, A. Elbourne, S. Walia, Antipathogenic properties and applications of low-dimensional materials, Nat. Commun. 12 (1) (2021) 3897.
[6] A. Elbourne, J. Chapman, A. Gelmi, D. Cozzolino, R.J. Crawford, V. Khanh Truong, Bacterial-nanostructure interactions: the role of cell elasticity and adhesion forces, J. Colloid Interface Sci. 546 (2019) 192–210.
[7] C.G. Pierce, T. Vila, J.A. Romo, D. Montelongo-Jauregui, G. Wall, A. Ramasubramanian, J.L. Lopez-Ribot, The Candida albicans Biofilm Matrix: Composition, Structure and Function, J. Fungi (Basel) 3 (1) (2017) 14.
[8] W.L. Chaffin, J.L. López-Ribot, M. Casanova, D. Gozalbo, J.P. Martínez, Cell wall and secreted proteins of Candida albicans: identification, function, and expression, Microbiol. Mol. Biol. Rev. 62 (1) (1998) 130–180.
[9] R. Garcia-Rubio, H.C. de Oliveira, J. Rivera, N. Trevijano-Contador, The Fungal Cell Wall: Candida, Cryptococcus, and Aspergillus Species, Front. Microbiol. 10 (2020) 2993.
[10] N.A. Gow, J.-P. Latge, C.A. Munro, The fungal cell wall: structure, biosynthesis, and function, The fungal kingdom (2017) 267–292.
[11] S. Cheeseman, A. Elbourne, S. Gangadoo, Z.L. Shaw, S.J. Bryant, N. Syed, M. D. Dickey, M.J. Higgins, K. Vasilev, C.F. McConville, A.J. Christofferson, R. J. Crawford, T. Daeneke, J. Chapman, V.K. Truong, Interactions between Liquid Metal Droplets and Bacterial, Fungal, and Mammalian Cells, Adv. Mater. Interfaces 9 (7) (2022) 2102113.
[12] S.M. Bowman, S.J. Free, The structure and synthesis of the fungal cell wall, Bioessays 28 (8) (2006) 799–808.
[13] R. Kariuki, R. Penman, S.J. Bryant, R. Orrell-Trigg, N. Meftahi, R.J. Crawford, C. F. McConville, G. Bryant, K. Voïtchovsky, C.E. Conn, A.J. Christofferson, A. Elbourne, Behavior of Citrate-Capped Ultrasmall Gold Nanoparticles on a Supported Lipid Bilayer Interface at Atomic Resolution, ACS Nano (2022).
[14] A. Albanese, W.C.W. Chan, Effect of Gold Nanoparticle Aggregation on Cell Uptake and Toxicity, ACS Nano 5 (7) (2011) 5478–5489.
[15] A. Sohrabi Kashani, K. Larocque, A. Piekny, M. Packirisamy, Gold Nano-Bio-Interaction to Modulate Mechanobiological Responses for Cancer Therapy Applications, ACS Appl. Bio Mater. (2022).
[16] G. Rossi, L. Monticelli, Gold nanoparticles in model biological membranes: A computational perspective, Biochim. Biophys. Acta (BBA) – Biomemb. 1858 (10) (2016) 2380–2389.
[17] P. Charchar, A.J. Christofferson, N. Todorova, I. Yarovsky, Gold Nanoparticles: Understanding and Designing the Gold-Bio Interface: Insights from Simulations (Small 18/2016), Small 12 (18) (2016) 2394.
[18] J.T. Wiemann, Z. Shen, H. Ye, Y. Li, Y. Yu, Membrane poration, wrinkling, and compression: deformations of lipid vesicles induced by amphiphilic Janus nanoparticles, Nanoscale 12 (39) (2020) 20326–20336.
[19] A. Banerjee, J. Qi, R. Gogoi, J. Wong, S. Mitragotri, Role of nanoparticle size, shape and surface chemistry in oral drug delivery, J. Control. Release 238 (2016) 176–185.
[20] N. Rispail, L. De Matteis, R. Santos, A.S. Miguel, L. Custardoy, P.S. Testillano, M. C. Risueño, A. Pérez-de-Luque, C. Maycock, P. Fevereiro, A. Oliva, R. Fernández-Pacheco, M.R. Ibarra, J.M. de la Fuente, C. Marquina, D. Rubiales, E. Prats, Quantum Dot and Superparamagnetic Nanoparticle Interaction with Pathogenic Fungi: Internalization and Toxicity Profile, ACS Appl. Mater. Interfaces 6 (12) (2014) 9100–9110.
[21] C. Formosa, M. Schiavone, H. Martin-Yken, J.M. François, R.E. Duval, E. Dague, Nanoscale Effects of Caspofungin against Two Yeast Species, Saccharomyces cerevisiae and Candida albicans, Antimicrob. Agents Chemother. 57 (8) (2013) 3498–3506.
[22] S. Pogodin, M. Werner, J.-U. Sommer, V.A. Baulin, Nanoparticle-Induced Permeability of Lipid Membranes, ACS Nano 6 (12) (2012) 10555–10561.
[23] S. Cheeseman, A.J. Christofferson, R. Kariuki, D. Cozzolino, T. Daeneke, R.J. Crawford, V.K. Truong, J. Chapman, A. Elbourne, Antimicrobial Metal Nanomaterials: From Passive to Stimuli-Activated Applications, Advanced Science n/a(n/a) (2020) 1902913.
[24] J. Shi, P.W. Kantoff, R. Wooster, O.C. Farokhzad, Cancer nanomedicine: progress, challenges and opportunities, Nat. Rev. Cancer 17 (1) (2017) 20–37.
[25] K.-H. Liao, Y.-S. Lin, C.W. Macosko, C.L. Haynes, Cytotoxicity of Graphene Oxide and Graphene in Human Erythrocytes and Skin Fibroblasts, ACS Appl. Mater. Interfaces 3 (7) (2011) 2607–2615.
[26] S. Li, N. Malmstadt, Deformation and poration of lipid bilayer membranes by cationic nanoparticles, Soft Matter 9 (20) (2013) 4969–4976.
[27] L. Li, S. Li, Y. Xu, L. Ren, L. Yang, X. Liu, Y. Dai, J. Zhao, T. Yue, Distinguishing the nanoplastic–cell membrane interface by polymer type and aging properties: translocation, transformation and perturbation, Environmental Science: Nano (2022).
[28] S.E.A. Gratton, P.A. Ropp, P.D. Pohlhaus, J.C. Luft, V.J. Madden, M.E. Napier, J. M. DeSimone, The effect of particle design on cellular internalization pathways, Proc. Natl. Acad. Sci. 105 (33) (2008) 11613–11618.
[29] T. Ahmad, I.A. Wani, I.H. Lone, A. Ganguly, N. Manzoor, A. Ahmad, J. Ahmed, A. S. Al-Shihri, Antifungal activity of gold nanoparticles prepared by solvothermal method, Mater. Res. Bull. 48 (1) (2013) 12–20.
[30] A. Lipovsky, Y. Nitzan, A. Gedanken, R. Lubart, Antifungal activity of ZnO nanoparticles—the role of ROS mediated cell injury, Nanotechnology 22 (10) (2011), 105101.
[31] S.M. El-sonbaty, F.S. Moawed, E.I. Kandil, A.M. Tamamm, Antitumor and Antibacterial Efficacy of Gallium Nanoparticles Coated by Ellagic Acid, Dose-Response 20 (1) (2022), 15593258211068998.
[32] L.Z.Y. Huang, A. Elbourne, Z.L. Shaw, S. Cheeseman, A. Goff, R. Orrell-Trigg, J. Chapman, B.J. Murdoch, R.J. Crawford, D. Friedmann, S.J. Bryant, V. K. Truong, R.A. Caruso, Dual-action silver functionalized nanostructured titanium against drug resistant bacterial and fungal species, J. Colloid Interface Sci. 628 (2022) 1049–1060.
[33] J.J. Artunduaga Bonilla, D.J. Paredes Guerrero, C.I. Sánchez Suárez, C.C. Ortiz López, R.G. Torres Sáez, In vitro antifungal activity of silver nanoparticles against fluconazole-resistant Candida species, World J. Microbiol. Biotechnol. 31 (11) (2015) 1801–1809.
[34] P.A. Arciniegas-Grijalba, M.C. Patiño-Portela, L.P. Mosquera-Sánchez, J. A. Guerrero-Vargas, J.E. Rodríguez-Páez, ZnO nanoparticles (ZnO-NPs) and their antifungal activity against coffee fungus Erythricium salmonicolor, Appl. Nanosci. 7 (5) (2017) 225–241.
[35] P.J. Molino, D. Yang, M. Penna, K. Miyazawa, B.R. Knowles, S. MacLaughlin, T. Fukuma, I. Yarovsky, M.J. Higgins, Hydration Layer Structure of Biofouling-Resistant Nanoparticles, ACS Nano 12 (11) (2018) 11610–11624.
[36] T. Sojinrin, J. Conde, K. Liu, J. Curtin, H.J. Byrne, D. Cui, F. Tian, Plasmonic gold nanoparticles for detection of fungi and human cutaneous fungal infections, Anal. Bioanal. Chem. 409 (2017) 4647–4658.
[37] J.I. Lee, S.C. Jang, J. Chung, W.-K. Choi, C. Hong, G.R. Ahn, S.H. Kim, B.Y. Lee, W.-J. Chung, Colorimetric allergenic fungal spore detection using peptide-modified gold nanoparticles, Sens. Actuators B 327 (2021), 128894.
[38] J.C. Ramirez-Perez, T.A. Reis, C.L. Olivera, M.A. Rizzutto, Impact of silver nanoparticles size on SERS for detection and identification of filamentous fungi, Spectrochim. Acta A Mol. Biomol. Spectrosc. 272 (2022), 120980.
[39] R. Etefagh, E. Azhir, N. Shahtahmasebi, Synthesis of CuO nanoparticles and fabrication of nanostructural layer biosensors for detecting Aspergillus niger fungi, Sci. Iran. 20 (3) (2013) 1055–1058.
[40] M.R. McGinnis, S.K. Tyring, Introduction to mycology, Medical Microbiology; Baron, S., Ed.; University of Texas Medical Branch at Galveston: Galveston, TX, USA (1996).
[41] J.W. Deacon, Modern mycology, Blackwell Science Oxford1997.
[42] H.W. Boucher, G.H. Talbot, J.S. Bradley, J.E. Edwards, D. Gilbert, L.B. Rice, M. Scheld, B. Spellberg, J. Bartlett, Bad Bugs, No Drugs: No ESKAPE! An Update from the Infectious Diseases Society of America, Clinical Infectious Diseases 48 (1) (2009) 1–12.
[43] B. Spellberg, R. Guidos, D. Gilbert, J. Bradley, H.W. Boucher, W.M. Scheld, J. G. Bartlett, J.J. Edwards, The Epidemic of Antibiotic-Resistant Infections: A Call to Action for the Medical Community from the Infectious Diseases Society of America, Clin. Infect. Dis. 46 (2) (2008) 155–164.
[44] K. Gulshan, W.S. Moye-Rowley, Multidrug resistance in fungi, Eukaryot. Cell 6 (11) (2007) 1933–1942.
[45] Z.L. Shaw, S. Kuriakose, S. Cheeseman, E.L.H. Mayes, A. Murali, Z.Y. Oo, T. Ahmed, N. Tran, K. Boyce, J. Chapman, C.F. McConville, R.J. Crawford, P. D. Taylor, A.J. Christofferson, V.K. Truong, M.J.S. Spencer, A. Elbourne, S. Walia, Broad-Spectrum Solvent-free Layered Black Phosphorus as a Rapid Action Antimicrobial, ACS Appl. Mater. Interfaces 13 (15) (2021) 17340–17352.
[46] Z.L. Shaw, S. Cheeseman, L.Z.Y. Huang, R. Penman, T. Ahmed, S.J. Bryant, G. Bryant, A.J. Christofferson, R. Orrell-Trigg, C. Dekiwadia, V.K. Truong, J. P. Vongsvivut, S. Walia, A. Elbourne, Illuminating the biochemical interaction of antimicrobial few-layer black phosphorus with microbial cells using synchrotron macro-ATR-FTIR, J. Mater. Chem. B (2022).
[47] E.J.J. Mallmann, F.A. Cunha, B.N.M.F. Castro, A.M. Maciel, E.A. Menezes, P.B. A. Fechine, Antifungal activity of silver nanoparticles obtained by green synthesis, Rev. Inst. Med. Trop. Sao Paulo 57 (2) (2015) 165–167.
[48] S.W. Kim, J.H. Jung, K. Lamsal, Y.S. Kim, J.S. Min, Y.S. Lee, Antifungal Effects of Silver Nanoparticles (AgNPs) against Various Plant Pathogenic Fungi, Mycobiology 40 (1) (2012) 53–58.
[49] C.S.O. Paulo, M. Vidal, L.S. Ferreira, Antifungal Nanoparticles and Surfaces, Biomacromolecules 11 (10) (2010) 2810–2817.

[50] T. Kruk, K. Szczepanowicz, J. Stefańska, R.P. Socha, P. Warszyński, Synthesis and antimicrobial activity of monodisperse copper nanoparticles, Colloids Surf. B Biointerfaces 128 (2015) 17–22.
[51] R. Brasseur, Y.F. Dufrêne, M. Deleu, M.-P. Mingeot-Leclercq, Atomic force microscopy of supported lipid bilayers, Nat. Protoc. 3 (10) (2008) 1654–1659.
[52] S.J. Marrink, V. Corradi, P.C.T. Souza, H.I. Ingólfsson, D.P. Tieleman, M.S. P. Sansom, Computational Modeling of Realistic Cell Membranes, Chem. Rev. 119 (9) (2019) 6184–6226.
[53] Y.F. Dufrêne, T. Ando, R. Garcia, D. Alsteens, D. Martinez-Martin, A. Engel, C. Gerber, D.J. Müller, Imaging modes of atomic force microscopy for application in molecular and cell biology, Nat. Nanotechnol. 12 (4) (2017) 295–307.
[54] D.J. Müller, Y.F. Dufrêne, Atomic force microscopy: a nanoscopic window on the cell surface, Trends Cell Biol. 21 (8) (2011) 461–469.
[55] P. Parot, Y.F. Dufrêne, P. Hinterdorfer, C. Le Grimellec, D. Navajas, J.-L. Pellequer, S. Scheuring, Past, present and future of atomic force microscopy in life sciences and medicine, J. Mol. Recognit. 20 (6) (2007) 418–431.
[56] Y. Shan, H. Wang, The structure and function of cell membranes examined by atomic force microscopy and single-molecule force spectroscopy, Chem. Soc. Rev. 44 (11) (2015) 3617–3638.
[57] G. Benn, A.L.B. Pyne, M.G. Ryadnov, B.W. Hoogenboom, Imaging live bacteria at the nanoscale: comparison of immobilisation strategies, Analyst (London) 144 (23) (2019) 6944–6952.
[58] R. Louise Meyer, X. Zhou, L. Tang, A. Arpanaei, P. Kingshott, F. Besenbacher, Immobilisation of living bacteria for AFM imaging under physiological conditions, Ultramicroscopy 110 (11) (2010) 1349–1357.
[59] L. Picas, F. Rico, S. Scheuring, Direct measurement of the mechanical properties of lipid phases in supported bilayers, Biophys. J . 102 (1) (2012) L01–L3.
[60] T. Jadidi, H. Seyyed-Allaei, M. Reza Tahimi Tabar, A. Mashaghi, Poisson's Ratio and Young's Modulus of Lipid Bilayers in Different Phases, Front. Bioeng. Biotechnol. 2 (2014) 8.
[61] C. Contini, J.W. Hindley, T.J. Macdonald, J.D. Barritt, O. Ces, N. Quirke, Size dependency of gold nanoparticles interacting with model membranes, Commun. Chem. 3 (1) (2020) 130.
[62] C. Formosa-Dague, R.E. Duval, E. Dague, Cell biology of microbes and pharmacology of antimicrobial drugs explored by Atomic Force Microscopy, Semin. Cell Dev. Biol. 73 (2018) 165–176.
[63] K.S. Siddiqi, A. Husen, Fabrication of Metal Nanoparticles from Fungi and Metal Salts: Scope and Application, Nanoscale Res. Lett. 11 (1) (2016) 98.
[64] P. Rauwel, S. Küünal, S. Ferdov, E. Rauwel, A Review on the Green Synthesis of Silver Nanoparticles and Their Morphologies Studied via TEM, Adv. Mater. Sci. Eng. 2015 (2015), 682749.
[65] M. Karkovska, O. Smutok, N. Stasyuk, M. Gonchar, L-Lactate-Selective Microbial Sensor Based On Flavocytochrome b2-Enriched Yeast Cells Using Recombinant And Nanotechnology Approaches, Talanta 144 (2015).
[66] J. Fan, M. Shao, L. Lai, Y. Liu, Z. Xie, Inhibition of autophagy contributes to the toxicity of cadmium telluride quantum dots in Saccharomyces cerevisiae, Int. J. Nanomed. 11 (2016) 3371–3383.
[67] H. Lara, G. Guisbiers, J. Mendoza, L. Mimun, B. Vincent, J. Lopez-Ribot, K. Nash, Synergistic antifungal effect of chitosan-stabilized selenium nanoparticles synthesized by pulsed laser ablation in liquids against Candida albicans biofilms, Int. J. Nanomed. 13 (2018) 2697–2708.
[68] K. Ishida, T. Cipriano, G. Rocha, G. Weissmuller, F. Gomes, K. Miranda, S. Rozental, Silver nanoparticle production by the fungus Fusarium oxysporum: Nanoparticle characterisation and analysis of antifungal activity against pathogenic yeasts, Mem. Inst. Oswaldo Cruz 109 (2012).
[69] S. Cheeseman, Z.L. Shaw, J. Vongsvivut, R.J. Crawford, M.F. dupont, K. Boyce, S. Gangadoo, S. Owen, S.J. Bryant, G. Bryant, D. Cozzolino, J. Chapman, A. Elbourne, V.K. Truong, Analysis of Pathogenic Bacterial and Fungal Biofilms using the Combination of Synchrotron ATR-FTIR Microspectroscopy and Chemometric approaches, Biofilm (2021).
[70] S.J. Parikh, J. Chorover, ATR-FTIR Spectroscopy Reveals Bond Formation During Bacterial Adhesion to Iron Oxide, Langmuir 22 (20) (2006) 8492–8500.
[71] J. Oberle, J. Dighton, G. Arbuckle-Keil, Comparison of methodologies for separation of fungal isolates using Fourier transform infrared (FTIR) spectroscopy and Fourier transform infrared-attenuated total reflectance (FTIR-ATR) microspectroscopy, Fungal Biol. 119 (11) (2015) 1100–1114.
[72] Z. Movasaghi, S. Rehman, D.I. ur Rehman, Fourier transform infrared (FTIR) spectroscopy of biological tissues, Appl. Spectrosc. Rev. 43 (2) (2008) 134–179.
[73] B.R. Wood, M.A. Quinn, F.R. Burden, D. McNaughton, An investigation into FTIR spectroscopy as a biodiagnostic tool for cervical cancer, Biospectroscopy 2 (3) (1996) 143–153.
[74] D. Hartnell, A. Hollings, A.M. Ranieri, H.B. Lamichhane, T. Becker, N.J. Sylvain, H. Hou, M.J. Pushie, E. Watkin, K.R. Bambery, Mapping sub-cellular protein aggregates and lipid inclusions using synchrotron ATR-FTIR microspectroscopy, Analyst (2021).
[75] D.Q. Pham, S.J. Bryant, S. Cheeseman, L.Z.Y. Huang, G. Bryant, M.F. Dupont, J. Chapman, C.C. Berndt, J. Vongsvivut, R.J. Crawford, V.K. Truong, A.S.M. Ang, A. Elbourne, Micro- to nano-scale chemical and mechanical mapping of antimicrobial-resistant fungal biofilms, Nanoscale 12 (38) (2020) 19888–19904.
[76] M.J. Hackett, F. Borondics, D. Brown, C. Hirschmugl, S.E. Smith, P.G. Paterson, H. Nichol, I.J. Pickering, G.N. George, Subcellular Biochemical Investigation of Purkinje Neurons Using Synchrotron Radiation Fourier Transform Infrared Spectroscopic Imaging with a Focal Plane Array Detector, ACS Chem. Nerosci. 4 (7) (2013) 1071–1080.
[77] J. Vongsvivut, D. Pérez-Guaita, B.R. Wood, P. Heraud, K. Khambatta, D. Hartnell, M.J. Hackett, M.J. Tobin, Synchrotron macro ATR-FTIR microspectroscopy for high-resolution chemical mapping of single cells, Analyst 144 (10) (2019) 3226–3238.
[78] N.A.R. Gow, M.D. Lenardon, Architecture of the dynamic fungal cell wall, Nat. Rev. Microbiol. 21 (4) (2023) 248–259.
[79] M. Gulati, C.J. Nobile, Candida albicans biofilms: development, regulation, and molecular mechanisms, Microbes Infect. 18 (5) (2016) 310–321.
[80] C.J. Nobile, A.D. Johnson, Candida albicans biofilms and human disease, Annu. Rev. Microbiol. 69 (2015) 71–92.
[81] J.V. Desai, A.P. Mitchell, D.R. Andes, Fungal biofilms, drug resistance, and recurrent infection, Cold Spring Harb. Perspect. Med. 4 (10) (2014), a019729.
[82] A. Beaussart, S. El-Kirat-Chatel, P. Herman, D. Alsteens, J. Mahillon, P. Hols, Yves F. Dufrêne, Single-Cell Force Spectroscopy of Probiotic Bacteria, Biophysical Journal 104(9) (2013) 1886-1892.
[83] S. Kang, M. Elimelech, Bioinspired single bacterial cell force spectroscopy, Langmuir 25 (17) (2009) 9656–9659.
[84] Z. Deng, W. Wang, X. Xu, Y. Nie, Y. Liu, O.E.C. Gould, N. Ma, A. Lendlein, Biofunction of Polydopamine Coating in Stem Cell Culture, ACS Appl. Mater. Interfaces 13 (9) (2021) 10748–10759.
[85] S. El-Kirat-Chatel, Y.F. Dufrêne, Nanoscale adhesion forces between the fungal pathogen Candida albicans and macrophages, Nanoscale Horiz. 1 (1) (2016) 69–74.
[86] D. Alsteens, A. Beaussart, S. Derclaye, S. El-Kirat-Chatel, H.R. Park, P.N. Lipke, Y. F. Dufrêne, Single-cell force spectroscopy of Als-mediated fungal adhesion, Anal. Methods 5 (15) (2013) 3657–3662.
[87] J.E. Sader, I. Larson, P. Mulvaney, L.R. White, Method for the calibration of atomic force microscope cantilevers, Rev. Sci. Instrum. 66 (7) (1995) 3789–3798.
[88] D. Nečas, P. Klapetek, Gwyddion: an open-source software for SPM data analysis, Open Physics (2012) 181.
[89] Biotium, Product information: yeast viability staining kit., Biotium, 2016.
[90] H. He, C. Xie, J. Ren, Nonbleaching fluorescence of gold nanoparticles and its applications in cancer cell imaging, Anal. Chem. 80 (15) (2008) 5951–5957.
[91] P. Rajapaksha, S. Cheeseman, S. Hombsch, B.J. Murdoch, S. Gangadoo, E. W. Blanch, Y. Truong, D. Cozzolino, C.F. McConville, R.J. Crawford, Antibacterial Properties of Graphene Oxide-Copper Oxide Nanoparticle Nanocomposites, ACS Appl. Bio Mater. 2 (12) (2019) 5687–5696.
[92] A. Elbourne, V.E. Coyle, V.K. Truong, Y.M. Sabri, A.E. Kandjani, S.K. Bhargava, E. P. Ivanova, R.J. Crawford, Multi-Directional Electrodeposited Gold Nanospikes for Antibacterial Surface Applications, Nanoscale Advances 1 (1) (2019) 203–212.
[93] S. Cheeseman, Z.L. Shaw, J. Vongsvivut, R.J. Crawford, M.F. Dupont, K.J. Boyce, S. Gangadoo, S.J. Bryant, G. Bryant, D. Cozzolino, J. Chapman, A. Elbourne, V. K. Truong, Analysis of Pathogenic Bacterial and Yeast Biofilms Using the Combination of Synchrotron ATR-FTIR Microspectroscopy and Chemometric Approaches, Molecules 26 (13) (2021) 3890.
[94] A.R. Spurr, A low-viscosity epoxy resin embedding medium for electron microscopy, J. Ultrastruct. Res. 26 (1–2) (1969) 31–43.
[95] D.P. Linklater, X. Le Guével, E. Kosyer, S. Rubanov, G. Bryant, E. Hanssen, V. A. Baulin, E. Pereiro, P.G.T. Perera, J.V. Wandiyanto, A. Angulo, S. Juodkazis, E. P. Ivanova, Functionalized Gold Nanoclusters Promote Stress Response in COS-7 Cells, Adv. NanoBiomed. Res. 3 (4) (2023) 2200102.
[96] P.G.T. Perera, Z. Vilagosh, D. Linklater, T.H.P. Nguyen, D. Appadoo, J. Vongsvivut, M. Tobin, C. Dekiwadia, R. Croft, E.P. Ivanova, Translocation and fate of nanospheres in pheochromocytoma cells following exposure to synchrotron-sourced terahertz radiation, J. Synchrotron Radiat. 30 (4) (2023).
[97] S. Cheeseman, V.K. Truong, J. Vongsvivut, M.J. Tobin, R. Crawford, E.P. Ivanova, Applications of synchrotron-source IR spectroscopy for the investigation of insect wings, Synchrotron Radiation, Intechopen2019.
[98] A. Savitzky, M.J.E. Golay, Smoothing and Differentiation of Data by Simplified Least Squares Procedures, Anal. Chem. 36 (8) (1964) 1627–1639.
[99] A. Kohler, C. Kirschner, A. Oust, H. Martens, Extended multiplicative signal correction as a tool for separation and characterization of physical and chemical information in Fourier transform infrared microscopy images of cryo-sections of beef loin, Appl. Spectrosc. 59 (6) (2005) 707–716.
[100] E. Correa, H. Sletta, D.I. Ellis, S. Hoel, H. Ertesvåg, T.E. Ellingsen, S. Valla, R. Goodacre, Rapid reagentless quantification of alginate biosynthesis in Pseudomonas fluorescens bacteria mutants using FT-IR spectroscopy coupled to multivariate partial least squares regression, Anal. Bioanal. Chem. 403 (9) (2012) 2591–2599.
[101] (!!! INVALID CITATION !!! [62, 63]).
[102] S. Zhu, Y. Shen, Y. Yu, X. Bai, Synthesis of antibacterial gold nanoparticles with different particle sizes using chlorogenic acid, R. Soc. Open Sci. 7 (3) (2020) 191141.
[103] Y. Yulizar, T. Utari, H.A. Ariyanta, D. Maulina, Green Method for Synthesis of Gold Nanoparticles Using Polyscias scutellaria Leaf Extract under UV Light and Their Catalytic Activity to Reduce Methylene Blue, J. Nanomater. 2017 (2017) 1–6.
[104] A.Y. Peleg, D.A. Hogan, E. Mylonakis, Medically important bacterial–fungal interactions, Nat. Rev. Microbiol. 8 (5) (2010) 340–349.
[105] A. Elbourne, S. Cheeseman, P. Atkin, N.P. Truong, N. Syed, A. Zavabeti, M. Mohiuddin, D. Esrafilzadeh, D. Cozzolino, C.F. McConville, M.D. Dickey, R. J. Crawford, K. Kalantar-Zadeh, J. Chapman, T. Daeneke, V.K. Truong, Antibacterial Liquid Metals: Biofilm Treatment via Magnetic Activation, ACS Nano (2020).
[106] P. Rajapaksha, S. Cheeseman, S. Hombsch, B.J. Murdoch, S. Gangadoo, E. W. Blanch, Y.B. Truong, D. Cozzolino, C.F. McConville, R.J. Crawford, V.

K. Truong, A. Elbourne, J. Chapman, Antibacterial Properties of Graphene Oxide-Copper Oxide Nanoparticle Nanocomposites, ACS Appl. Bio Mater. (2019).
[107] S. Cheeseman, A. Elbourne, R. Kariuki, A.V. Ramarao, A. Zavabeti, N. Syed, A. J. Christofferson, K.Y. Kwon, W. Jung, M.D. Dickey, K. Kalantar-Zadeh, C. F. McConville, R.J. Crawford, T. Daeneke, J. Chapman, V.K. Truong, Broad-spectrum treatment of bacterial biofilms using magneto-responsive liquid metal particles, J. Mater. Chem. B 8 (47) (2020) 10776–10787.
[108] A. Elbourne, V.K. Truong, S. Cheeseman, P. Rajapaksha, S. Gangadoo, J. Chapman, R.J. Crawford, The use of nanomaterials for the mitigation of pathogenic biofilm formation, Methods in Microbiology, Academic Press2019.
[109] P. Pallavicini, A. Donà, A. Taglietti, P. Minzioni, M. Patrini, G. Dacarro, G. Chirico, L. Sironi, N. Bloise, L. Visai, L. Scarabelli, Self-assembled monolayers of gold nanostars: A convenient tool for near-IR photothermal biofilm eradication, Chem. Commun. (Camb) 50 (16) (2014) 1969–1971.
[110] C.P. Teng, T. Zhou, E. Ye, S. Liu, L.D. Koh, M. Low, X.J. Loh, K.Y. Win, L. Zhang, M.Y. Han, Effective Targeted Photothermal Ablation of Multidrug Resistant Bacteria and Their Biofilms with NIR-Absorbing Gold Nanocrosses, Adv. Healthc. Mater. 5 (16) (2016) 2122–2130.
[111] D. Pissuwan, C.H. Cortie, S.M. Valenzuela, M.B. Cortie, Functionalised gold nanoparticles for controlling pathogenic bacteria, Trends Biotechnol. 28 (4) (2010) 207–213.
[112] P.M. Tiwari, K. Vig, V.A. Dennis, S.R. Singh, Functionalized Gold Nanoparticles and Their Biomedical Applications, Nanomaterials 1 (1) (2011) 31–63.
[113] S. Kalita, R. Kandimalla, K.K. Sharma, A.C. Kataki, M. Deka, J. Kotoky, Amoxicillin functionalized gold nanoparticles reverts MRSA resistance, Mater. Sci. Eng. C 61 (2016) 720–727.
[114] L. Chopinet, C. Formosa, M. Rols, R. Duval, E. Dague, Imaging living cells surface and quantifying its properties at high resolution using AFM in QI™ mode, Micron 48 (2013) 26–33.
[115] S. Ma, W. Ge, Y. Yan, X. Huang, L. Ma, C. Li, S. Yu, C. Chen, Effects of Streptococcus sanguinis Bacteriocin on DeformationAdhesion Ability, and Young's Modulus of Candida albicans, BioMed. Res. Int. 2017 (2017) 5291486–5291488.
[116] D. Alsteens, M.C. Garcia, P.N. Lipke, Y.F. Dufrêne, Force-induced formation and propagation of adhesion nanodomains in living fungal cells, Proceedings of the National Academy of Sciences - PNAS 107(48) (2010) 20744-20749.
[117] A.K. Tyagi, A. Malik, In situ SEM, TEM and AFM studies of the antimicrobial activity of lemon grass oil in liquid and vapour phase against Candida albicans, Micron (Oxford, England : 1993) 41(7) (2010) 797-805.
[118] V.M. Laurent, R. Michel, A. Duperray, C. Verdier, Microrheology of complex systems and living cells using AFM, Comput. Methods Biomech. Biomed. Eng. 16 (supp1) (2013) 15–16.
[119] M.D.A. Norman, S.A. Ferreira, G.M. Jowett, L. Bozec, E. Gentleman, Measuring the elastic modulus of soft culture surfaces and three-dimensional hydrogels using atomic force microscopy, Nat. Protoc. 16 (5) (2021) 2418–2449.
[120] Y. Abidine, V.M. Laurent, R. Michel, A. Duperray, L.I. Palade, C. Verdier, Physical properties of polyacrylamide gels probed by AFM and rheology, Europhys. Lett. 109 (3) (2015) 38003.
[121] Y.H. Chim, L.M. Mason, N. Rath, M.F. Olson, M. Tassieri, H. Yin, A one-step procedure to probe the viscoelastic properties of cells by Atomic Force Microscopy, Sci. Rep. 8 (1) (2018) 1–12.
[122] K. Gnanachandran, S. Kedracka-Krok, J. Pabijan, M. Lekka, Nanomechanical and microrheological properties of bladder cancer cells at cellular and spheroid levels, bioRxiv (2022) 2022.03. 21.485153.
[123] J. Alcaraz, L. Buscemi, M. Grabulosa, X. Trepat, B. Fabry, R. Farré, D. Navajas, Microrheology of Human Lung Epithelial Cells Measured by Atomic Force Microscopy, Biophys. J . 84 (3) (2003) 2071–2079.
[124] S.G.W. Kaminskyj, T.E.S. Dahms, High spatial resolution surface imaging and analysis of fungal cells using SEM and AFM, Micron 39 (4) (2008) 349–361.
[125] L. Zhao, D. Schaefer, H. Xu, S.J. Modi, W.R. LaCourse, M.R. Marten, Elastic properties of the cell wall of Aspergillus nidulans studied with atomic force microscopy, Biotechnol. Prog. 21 (1) (2005) 292–299.
[126] P.H. Le, D.H.K. Nguyen, A.A. Medina, D.P. Linklater, C. Loebbe, R.J. Crawford, S. MacLaughlin, E.P. Ivanova, Surface Architecture Influences the Rigidity of Candida albicans Cells, Nanomaterials 12 (3) (2022) 567.
[127] F. Pillet, S. Lemonier, M. Schiavone, C. Formosa, H. Martin-Yken, J.M. Francois, E. Dague, Uncovering by Atomic Force Microscopy of an original circular structure at the yeast cell surface in response to heat shock, BMC Biol. 12 (1) (2014) 6.
[128] M. Schiavone, C. Formosa-Dague, C. Elsztein, M.-A. Teste, H. Martin-Yken, M.A. D. Morais, E. Dague, J.M. François, Evidence for a Role for the Plasma Membrane in the Nanomechanical Properties of the Cell Wall as Revealed by an Atomic Force Microscopy Study of the Response of Saccharomyces cerevisiae to Ethanol Stress, Appl. Environ. Microbiol. 82 (15) (2016) 4789–4801.
[129] S. Gonçalves, P.M. Silva, M.R. Felício, L.N. de Medeiros, E. Kurtenbach, N. C. Santos, Ps d1 Effects on Candida albicans planktonic cells and biofilms, Front. Cell. Infect. Microbiol. 7 (2017) 249.
[130] W. Jiang, A. Saxena, B. Song, B.B. Ward, T.J. Beveridge, S.C.B. Myneni, Elucidation of Functional Groups on Gram-Positive and Gram-Negative Bacterial Surfaces Using Infrared Spectroscopy, Langmuir 20 (26) (2004) 11433–11442.
[131] J. Vongsvivut, P. Heraud, A. Gupta, M. Puri, D. McNaughton, C.J. Barrow, FTIR microspectroscopy for rapid screening and monitoring of polyunsaturated fatty acid production in commercially valuable marine yeasts and protists, Analyst 138 (20) (2013) 6016–6031.
[132] S. Cheeseman, Z.L. Shaw, J. Vongsvivut, R.J. Crawford, M.F. Dupont, K.J. Boyce, S. Gangadoo, S.J. Bryant, G. Bryant, D. Cozzolino, J. Chapman, A. Elbourne, V.K. Truong, Analysis of pathogenic bacterial and yeast biofilms using the combination of synchrotron ATR-FTIR microspectroscopy and chemometric approaches, Molecules (Basel, Switzerland) 26(13) (2021) 3890.
[133] S. Kaminskyj, K. Jilkine, A. Szeghalmi, K. Gough, High spatial resolution analysis of fungal cell biochemistry – bridging the analytical gap using synchrotron FTIR spectromicroscopy, FEMS Microbiol. Lett. 284 (1) (2008) 1–8.
[134] V. Farkas, Biosynthesis of cell walls of fungi, Microbiol. Rev. 43 (2) (1979) 117–144.
[135] S. Fanning, A.P. Mitchell, Fungal Biofilms, PLoS Pathog. 8 (4) (2012) e1002585.
[136] K.F. Mitchell, R. Zarnowski, D.R. Andes, The Extracellular Matrix of Fungal Biofilms, in: C. Imbert (Ed.), Fungal Biofilms and related infections: Advances in Microbiology, Infectious Diseases and Public Health, Volume 3, Springer International Publishing, Cham, 2016, pp. 21–35.
[137] K.F. Mitchell, R. Zarnowski, D.R. Andes, Fungal Super Glue: The Biofilm Matrix and Its Composition, Assembly, and Functions, PLoS Pathog. 12 (9) (2016) e1005828.
[138] H.A. Wösten, Hydrophobins: multipurpose proteins, Ann. Rev. Microbiol. 55 (1) (2001) 625–646.
[139] S. Wold, K. Esbensen, P. Geladi, Principal component analysis, Chemom. Intel. Lab. Syst. 2 (1–3) (1987) 37–52.
[140] S.J. Bryant, Z.L. Shaw, L.Z.Y. Huang, A. Elbourne, A.N. Abraham, J. Vongsvivut, S.A. Holt, T.L. Greaves, G. Bryant, Insights into Chemical Interactions and Related Toxicities of Deep Eutectic Solvents with Mammalian Cells Observed Using Synchrotron Macro–ATR–FTIR Microspectroscopy, Biophysica 3 (2) (2023) 318–334.
[141] E. Lipiec, K.R. Bambery, P. Heraud, C. Hirschmugl, J. Lekki, W.M. Kwiatek, M. J. Tobin, C. Vogel, D. Whelan, B.R. Wood, Synchrotron FTIR shows evidence of DNA damage and lipid accumulation in prostate adenocarcinoma PC-3 cells following proton irradiation, J. Mol. Struct. 1073 (2014) 134–141.
[142] K.-J. Kim, W.S. Sung, S.-K. Moon, J.-S. Choi, J.G. Kim, D.G. Lee, Antifungal effect of silver nanoparticles on dermatophytes, J. Microbiol. Biotechnol. 18 (8) (2008) 1482–1484.
[143] A. Nasrollahi, K. Pourshamsian, P. Mansourkiaee, Antifungal activity of silver nanoparticles on some of fungi, (2011).
[144] D. Sharma, J. Rajput, B. Kaith, M. Kaur, S. Sharma, Synthesis of ZnO nanoparticles and study of their antibacterial and antifungal properties, Thin Solid Films 519 (3) (2010) 1224–1229.
[145] L. Yien, N.M. Zin, A. Sarwar, H. Katas, Antifungal activity of chitosan nanoparticles and correlation with their physical properties, Int. J. Biomater. 2012 (2012).
[146] M. Guilger-Casagrande, R.d. Lima, Synthesis of silver nanoparticles mediated by fungi: a review, Frontiers in bioengineering and biotechnology 7 (2019) 287.
[147] D. MubarakAli, N. Thajuddin, K. Jeganathan, M. Gunasekaran, Plant extract mediated synthesis of silver and gold nanoparticles and its antibacterial activity against clinically isolated pathogens, Colloids Surf. B Biointerfaces 85 (2) (2011) 360–365.
[148] L. Wang, C. Hu, L. Shao, The antimicrobial activity of nanoparticles: present situation and prospects for the future, Int. J. Nanomed. 12 (2017) 1227–1249.
[149] S.M. Dizaj, F. Lotfipour, M. Barzegar-Jalali, M.H. Zarrintan, K. Adibkia, Antimicrobial activity of the metals and metal oxide nanoparticles, Mater. Sci. Eng. C 44 (2014) 278–284.
[150] G. Ramesh, J.E. Kaviyil, W. Paul, R. Sasi, R. Joseph, Gallium-Curcumin Nanoparticle Conjugates as an Antibacterial Agent against Pseudomonas aeruginosa: Synthesis and Characterization, ACS Omega 7 (8) (2022) 6795–6809.
[151] S. Dwivedi, R. Wahab, F. Khan, Y.K. Mishra, J. Musarrat, A.A. Al-Khedhairy, Reactive Oxygen Species Mediated Bacterial Biofilm Inhibition via Zinc Oxide Nanoparticles and Their Statistical Determination, PLoS One 9 (11) (2014) e111289.
[152] I. Anghel, A. Grumezescu, A. Holban, A. Ficai, A. Anghel, M. Chifiriuc, Biohybrid Nanostructured Iron Oxide Nanoparticles and Satureja hortensis to Prevent Fungal Biofilm Development, Int. J. Mol. Sci. 14 (9) (2013) 18110.
[153] F. Haghighi, S. Roudbar Mohammadi, P. Mohammadi, S. Hosseinkhani, R. Shipour, Antifungal activity of TiO2 nanoparticles and EDTA on Candida albicans biofilms, Infection, Epidemiol. Microbiol. 1 (1) (2013) 33–38.
[154] F. Natalio, R. André, A.F. Hartog, B. Stoll, K.P. Jochum, R. Wever, W. Tremel, Vanadium pentoxide nanoparticles mimic vanadium haloperoxidases and thwart biofilm formation, Nat. Nanotechnol. 7 (8) (2012) 530.
[155] C. Marambio-Jones, E.M.V. Hoek, A review of the antibacterial effects of silver nanomaterials and potential implications for human health and the environment, J. Nanopart. Res. 12 (5) (2010) 1531–1551.
[156] I. Sondi, B. Salopek-Sondi, Silver nanoparticles as antimicrobial agent: a case study on E. coli as a model for Gram-negative bacteria, J. Colloid Interface Sci. 275 (1) (2004) 177–182.
[157] S. Meghana, P. Kabra, S. Chakraborty, N. Padmavathy, Understanding the pathway of antibacterial activity of copper oxide nanoparticles, RSC Adv. 5 (16) (2015) 12293–12299.
[158] A.K. Chatterjee, R. Chakraborty, T. Basu, Mechanism of antibacterial activity of copper nanoparticles, Nanotechnology 25 (13) (2014), 135101.
[159] J. Ramyadevi, K. Jeyasubramanian, A. Marikani, G. Rajakumar, A.A. Rahuman, Synthesis and antimicrobial activity of copper nanoparticles, Mater. Lett. 71 (2012) 114–116.
[160] S. Jadhav, S. Gaikwad, M. Nimse, A. Rajbhoj, Copper Oxide Nanoparticles: Synthesis, Characterization and Their Antibacterial Activity, J. Clust. Sci. 22 (2) (2011) 121–129.
[161] G.R.d.S. Araújo, N.B. Viana, F. Gómez, B. Pontes, S. Frases, The mechanical properties of microbial surfaces and biofilms, The Cell Surface 5 (2019), 100028.

[162] C. Picioreanu, F. Blauert, H. Horn, M. Wagner, Determination of mechanical properties of biofilms by modelling the deformation measured using optical coherence tomography, Water Res. 145 (2018) 588–598.
[163] V. Carniello, B.W. Peterson, H.C. van der Mei, H.J. Busscher, Physico-chemistry from initial bacterial adhesion to surface-programmed biofilm growth, Adv. Colloid Interface Sci. 261 (2018) 1–14.
[164] C.B. Costa-Orlandi, J.C.O. Sardi, N.S. Pitangui, H.C. de Oliveira, L. Scorzoni, M. C. Galeane, K.P. Medina-Alarcón, W.C.M.A. Melo, M.Y. Marcelino, J.D. Braz, A. M. Fusco-Almeida, M.J.S. Mendes-Giannini, Fungal Biofilms and Polymicrobial Diseases, J. Fungi (Basel) 3 (2) (2017) 22.
[165] D. Septiadi, F. Crippa, T.L. Moore, B. Rothen-Rutishauser, A. Petri-Fink, Nanoparticle-Cell Interaction: A Cell Mechanics Perspective, Adv. Mater. 30 (19) (2018) 1704463.
[166] S. Zhang, H. Gao, G. Bao, Physical Principles of Nanoparticle Cellular Endocytosis, ACS Nano 9 (9) (2015) 8655–8671.
[167] M.A.I. Rasel, S. Singh, T.D. Nguyen, I.O. Afara, Y. Gu, Impact of Nanoparticle Uptake on the Biophysical Properties of Cell for Biomedical Engineering Applications, Sci. Rep. 9 (1) (2019) 5859.
[168] C. Carnovale, G. Bryant, R. Shukla, V. Bansal, Size, shape and surface chemistry of nano-gold dictate its cellular interactions, uptake and toxicity, Prog. Mater Sci. 83 (2016) 152–190.
[169] C. Carnovale, G. Bryant, R. Shukla, V. Bansal, Identifying trends in gold nanoparticle toxicity and uptake: size, shape, capping ligand, and biological corona, ACS Omega 4 (1) (2019) 242–256.
[170] D.P. Linklater, X. Le Guével, G. Bryant, V.A. Baulin, E. Pereiro, P.G.T. Perera, J. V. Wandiyanto, S. Juodkazis, E.P. Ivanova, Lethal Interactions of Atomically Precise Gold Nanoclusters and Pseudomonas aeruginosa and Staphylococcus aureus Bacterial Cells, ACS Appl. Mater. Interfaces 14 (28) (2022) 32634–32645.
[171] R. Augustine, A. Hasan, R. Primavera, R.J. Wilson, A.S. Thakor, B.D. Kevadiya, Cellular uptake and retention of nanoparticles: Insights on particle properties and interaction with cellular components, Mater. Today Commun. 25 (2020), 101692.
[172] P. Foroozandeh, A.A. Aziz, Insight into Cellular Uptake and Intracellular Trafficking of Nanoparticles, Nanoscale Res. Lett. 13 (1) (2018) 339.
[173] T. Zhang, L. Wang, Q. Chen, C. Chen, Cytotoxic potential of silver nanoparticles, Yonsei Med. J. 55 (2) (2014) 283–291.
[174] K.-N. Yu, T.-J. Yoon, A. Minai-Tehrani, J.-E. Kim, S.J. Park, M.S. Jeong, S.-W. Ha, J.-K. Lee, J.S. Kim, M.-H. Cho, Zinc oxide nanoparticle induced autophagic cell death and mitochondrial damage via reactive oxygen species generation, Toxicol. In Vitro 27 (4) (2013) 1187–1195.
[175] W. Song, J. Zhang, J. Guo, J. Zhang, F. Ding, L. Li, Z. Sun, Role of the dissolved zinc ion and reactive oxygen species in cytotoxicity of ZnO nanoparticles, Toxicol. Lett. 199 (3) (2010) 389–397.
[176] I.-S. Kim, M. Baek, S.-J. Choi, Comparative Cytotoxicity of Al2O3, CeO2, TiO2 and ZnO Nanoparticles to Human Lung Cells, J. Nanosci. Nanotechnol. 10 (5) (2010) 3453–3458.
[177] Y. Pan, S. Neuss, A. Leifert, M. Fischler, F. Wen, U. Simon, G. Schmid, W. Brandau, W. Jahnen-Dechent, Size-dependent cytotoxicity of gold nanoparticles, Small 3 (11) (2007) 1941–1949.
[178] J. Ren, N. Andrikopoulos, K. Velonia, H. Tang, R. Cai, F. Ding, P.C. Ke, C. Chen, Chemical and Biophysical Signatures of the Protein Corona in Nanomedicine, J. Am. Chem. Soc. 144 (21) (2022) 9184–9205.
[179] P. Singh, S. Pandit, V.R.S.S. Mokkapati, A. Garg, V. Ravikumar, I. Mijakovic, Gold Nanoparticles in Diagnostics and Therapeutics for Human Cancer, Int. J. Mol. Sci. 19 (7) (2018) 1979.
[180] A. Elbourne, R.J. Crawford, E.P. Ivanova, Nano-structured antimicrobial surfaces: From nature to synthetic analogues, J. Colloid Interface Sci. (2017).
[181] S.K. Murthy, Nanoparticles in modern medicine: state of the art and future challenges, Int. J. Nanomed. 2 (2) (2007) 129–141.
[182] C. Contini, M. Schneemilch, S. Gaisford, N. Quirke, Nanoparticle–membrane interactions, J. Exp. Nanosci. 13 (1) (2018) 62–81.
[183] J.R. Nicol, D. Dixon, J.A. Coulter, Gold nanoparticle surface functionalization: a necessary requirement in the development of novel nanotherapeutics, Nanomedicine (Lond.) 10 (8) (2015) 1315–1326.
[184] Q. Zhang, Y. Gong, X.-J. Guo, P. Zhang, C.-F. Ding, Multifunctional Gold Nanoparticle-Based Fluorescence Resonance Energy-Transfer Probe for Target Drug Delivery and Cell Fluorescence Imaging, ACS Appl. Mater. Interfaces 10 (41) (2018) 34840–34848.
[185] E. Hinde, K. Thammasiraphop, H.T.T. Duong, J. Yeow, B. Karagoz, C. Boyer, J. J. Gooding, K. Gaus, Pair correlation microscopy reveals the role of nanoparticle shape in intracellular transport and site of drug release, Nat. Nanotechnol. 12 (1) (2017) 81–89.
[186] M.A.I. Rasel, T. Li, T.D. Nguyen, S. Singh, Y. Zhou, Y. Xiao, Y. Gu, Biophysical response of living cells to boron nitride nanoparticles: uptake mechanism and bio-mechanical characterization, J. Nanopart. Res. 17 (11) (2015) 441.
[187] A. Bhat, K. Huan, T. Cooks, H. Boukari, Q. Lu, Probing Interactions between AuNPs/AgNPs and Giant Unilamellar Vesicles (GUVs) Using Hyperspectral Dark-field Microscopy, Int. J. Mol. Sci. 19 (4) (2018) 1014.
[188] R.C. Van Lehn, P.U. Atukorale, R.P. Carney, Y.-S. Yang, F. Stellacci, D.J. Irvine, A. Alexander-Katz, Effect of Particle Diameter and Surface Composition on the Spontaneous Fusion of Monolayer-Protected Gold Nanoparticles with Lipid Bilayers, Nano Lett. 13 (9) (2013) 4060–4067.
[189] C. Contini, J. Hindley, T. Macdonald, J. Barritt, O. Ces, N. Quirke, Size matters: Size Dependency of Gold Nanoparticles Interacting with Model Membranes, ChemRxiv (2019).
[190] A. Ridolfi, L. Caselli, C. Montis, G. Mangiapia, D. Berti, M. Brucale, F. Valle, Gold nanoparticles interacting with synthetic lipid rafts: an AFM investigation, J. Microsc. 280 (3) (2020) 194–203.
[191] J.M. Troiano, L.L. Olenick, T.R. Kuech, E.S. Melby, D. Hu, S.E. Lohse, A. C. Mensch, M. Dogangun, A.M. Vartanian, M.D. Torelli, E. Ehimiaghe, S. R. Walter, L. Fu, C.R. Anderton, Z. Zhu, H. Wang, G. Orr, C.J. Murphy, R. J. Hamers, J.A. Pedersen, F.M. Geiger, Direct Probes of 4 nm Diameter Gold Nanoparticles Interacting with Supported Lipid Bilayers, J. Phys. Chem. C 119 (1) (2015) 534–546.
[192] N. Sakaguchi, Y. Kimura, A. Hirano-Iwata, T. Ogino, Fabrication of Au-Nanoparticle-Embedded Lipid Bilayer Membranes Supported on Solid Substrates, J. Phys. Chem. B 121 (17) (2017) 4474–4481.
[193] Y. Bunga, R. Kataky, Real time monitoring of interactions of gold nanoparticles with supported phospholipid lipid layers, J. Electroanal. Chem. 872 (2020), 114302.
[194] X. Lin, C. Wang, M. Wang, K. Fang, N. Gu, Computer Simulation of the Effects of Nanoparticles' Adsorption on the Properties of Supported Lipid Bilayer, J. Phys. Chem. C 116 (33) (2012) 17960–17968.
[195] X. Wang, X. Wang, X. Bai, L. Yan, T. Liu, M. Wang, Y. Song, G. Hu, Z. Gu, Q. Miao, C. Chen, Nanoparticle Ligand Exchange and Its Effects at the Nanoparticle-Cell Membrane Interface, Nano Lett. 19 (1) (2019) 8–18.
[196] C. Xing, R. Faller, Interactions of Lipid Bilayers with Supports: A Coarse-Grained Molecular Simulation Study, J. Phys. Chem. B 112 (23) (2008) 7086–7094.
[197] A.R. Mhashal, S. Roy, Effect of Gold Nanoparticle on Structure and Fluidity of Lipid Membrane, PLoS One 9 (12) (2014) e114152.
[198] S. Salassi, L. Caselli, J. Cardellini, E. Lavagna, C. Montis, D. Berti, G. Rossi, A Martini Coarse Grained Model of Citrate-Capped Gold Nanoparticles Interacting with Lipid Bilayers, J. Chem. Theory Comput. 17 (10) (2021) 6597–6609.
[199] R. Gupta, B. Rai, Effect of Size and Surface Charge of Gold Nanoparticles on their Skin Permeability: A Molecular Dynamics Study, Sci. Rep. 7 (1) (2017) 45292.
[200] J. Cardellini, L. Caselli, E. Lavagna, S. Salassi, H. Amenitsch, M. Calamai, C. Montis, G. Rossi, D. Berti, Membrane Phase Drives the Assembly of Gold Nanoparticles on Biomimetic Lipid Bilayers, J. Phys. Chem. C 126 (9) (2022) 4483–4494.
[201] X. Lin, X. Lin, N. Gu, Optimization of hydrophobic nanoparticles to better target lipid rafts with molecular dynamics simulations, Nanoscale 12 (6) (2020) 4101–4109.
[202] T. Pfeiffer, A. De Nicola, C. Montis, F. Carlà, N.F. van der Vegt, D. Berti, G. Milano, Nanoparticles at biomimetic interfaces: combined experimental and simulation study on charged gold nanoparticles/lipid bilayer interfaces, J. Phys. Chem. Lett. 10 (2) (2018) 129–137.
[203] K.R. Hossain, D.R. Turkewitz, S.A. Holt, A.P. Le Brun, S.M. Valenzuela, Sterol Structural Features' Impact on the Spontaneous Membrane Insertion of CLIC1 into Artificial Lipid Membranes, Langmuir 39 (9) (2023) 3286–3300.
[204] Z. Al-Rekabi, S. Contera, Multifrequency AFM reveals lipid membrane mechanical properties and the effect of cholesterol in modulating viscoelasticity. Proceedings of the National Academy of Sciences, 2018.
[205] S.T. Yang, A.J.B. Kreutzberger, J. Lee, V. Kiessling, L.K. Tamm, The role of cholesterol in membrane fusion, Chem. Phys. Lipids 199 (2016) 136–143.
[206] C. Ibe, C.A. Munro, Fungal Cell Wall Proteins and Signaling Pathways Form a Cytoprotective Network to Combat Stresses, J. Fungi (Basel) 7 (9) (2021).
[207] W.L. Chaffin, Cell Wall of Human Fungal Pathogens and its Interaction with Host Extracellular Matrix, in: R.J. Howard, N.A.R. Gow (Eds.), Biology of the Fungal Cell, Springer, Berlin Heidelberg, Berlin, Heidelberg, 2001, pp. 161–180.
[208] J. Grouleff, S.J. Irudayam, K.K. Skeby, B. Schiøtt, The influence of cholesterol on membrane protein structure, function, and dynamics studied by molecular dynamics simulations, Biochim. Biophys. Acta (BBA) – Biomemb. 1848 (9) (2015) 1783–1795.
[209] O. Hollóczki, S. Gehrke, Can Nanoplastics Alter Cell Membranes? ChemPhysChem 21 (1) (2020) 9–12.
[210] B. Geny, M.R. Popoff, Bacterial protein toxins and lipids: pore formation or toxin entry into cells, Biol. Cell 98 (11) (2006) 667–678.
[211] C. Soliman, S. Eastwood, V.K. Truong, P.A. Ramsland, A. Elbourne, The membrane effects of melittin on gastric and colorectal cancer, PLoS One 14 (10) (2019) e0224028.
[212] T.O. Paiva, A. Viljoen, Y.F. Dufrêne, Seeing the unseen: High-resolution AFM imaging captures antibiotic action in bacterial membranes, Nat. Commun. 13 (1) (2022) 6196.
[213] S.L. Lima, A.L. Colombo, J.N. de Almeida Junior, Fungal Cell Wall: Emerging Antifungals and Drug Resistance, Front. Microbiol. 10 (2019).
[214] A. Hopke, A.J.P. Brown, R.A. Hall, R.T. Wheeler, Dynamic Fungal Cell Wall Architecture in Stress Adaptation and Immune Evasion, Trends Microbiol. 26 (4) (2018) 284–295.
[215] S.J. Bryant, M.N. Awad, A. Elbourne, A.J. Christofferson, A.V. Martin, N. Meftahi, C.J. Drummond, T.L. Greaves, G. Bryant, Deep eutectic solvents as cryoprotective agents for mammalian cells, J. Mater. Chem. B 10 (24) (2022) 4546–4560.
[216] B.P. Dyett, H. Yu, J. Strachan, C.J. Drummond, C.E. Conn, Fusion dynamics of cubosome nanocarriers with model cell membranes, Nat. Commun. 10 (1) (2019) 1–13.
[217] S.A.A. Rizvi, A.M. Saleh, Applications of nanoparticle systems in drug delivery technology, Saudi Pharm J 26 (1) (2018) 64–70.
[218] N. Oh, J.-H. Park, Surface Chemistry of Gold Nanoparticles Mediates Their Exocytosis in Macrophages, ACS Nano 8 (6) (2014) 6232–6241.